The Local Environments of Low-Redshift Supernovae

Research Thesis

Presented in Partial Fulfillment of the Requirements for graduation *with research distinction* in Astronomy and Astrophysics in the undergraduate colleges of The Ohio State University

by

Serena A. Cronin

The Ohio State University

December 2020

Project Advisors: Dr. Adam Leroy[1] & Dr. Dyas Utomo[2,1]
[1]Department of Astronomy
[2]The National Radio Astronomy Observatory

Abstract

I aimed to characterize the local (∼2 kpc) environments of Type Ia, II, and Ibc supernovae (SNe) by measuring the ultraviolet (UV) and infrared (IR) emission at supernova (SN) sites. Measuring the amount of host galaxy emission at SN sites gives insight into their progenitor population and allows one to search for consistency between the star formation rate and the SN rate. Starting with an atlas of ∼16,000 local (d $\lesssim$ 50 Mpc) galaxies, I selected 472 SNe that occurred in 359 low-inclination, nearby galaxies using The Open Supernova Catalog. I located each SN in UV and IR images that highlight regions of young stars, old stars, and dust. These images were observed by NASA's *GALEX* and WISE missions. I sought to test the hypothesis that Type Ia SNe (SNe Ia) track the starlight of their host galaxies, whereas core-collapse SNe, which are Type II (SNe II) and Type Ibc (SNe Ibc), are tightly linked to regions of young stars and active star formation. Following previous works, I adopted a pixel statistics method to generate cumulative distribution functions (CDFs) of UV and IR emission within a 2 kpc region of the explosion site for each SN type. I found that, generally, SNe Ia follow near-IR (W1) light, which traces the total distribution of all stars in a galaxy. SNe II are distributed like that of a combination of mid-IR (W4) and far-UV (FUV) emission that traces recent star formation. SNe Ibc appear to track emission from small, hot dust grains as traced by W3 emission. Finally, I estimated that the SN rate for galaxies with $d < 50$ Mpc and $i \leq 60°$ is $0.4 - 2.3$ SNe per 100 years per 10^{10} $M_\odot$ and $0.7 - 2.1$ SNe per 100 years per $M_\odot$ yr^{-1}, which is in line with the observed rate for the Milky Way. The work of this thesis is also presented in the paper Cronin et al. (2021, *in prep.*), and my Python programs can be found at github.com/serc7.

Acknowledgements

This work has been partially supported by NASA ADAP grant NNX16AF48G and The Ohio State University's College of Arts and Sciences Undergraduate Research Scholarship. In addition, I would like to give a special thank you to:

1. My project advisors, Dr. Dyas Utomo and Dr. Adam Leroy, for taking me on as a student and introducing me to research.
2. My thesis committee, Dr. Adam Leroy and Dr. Laura Lopez, for helping me through the thesis process.
3. Dr. Wayne Schlingman for an immense amount of help and support over the years.
4. The Department of Astronomy Summer Undergraduate Research Program (SURP).

Contents

Chapter 1

Introduction

As stars evolve, some will explode in a violent death called a supernova (SN). Supernovae (SNe) are responsible for creating the heavy elements that now enrich the Universe. They also have catastrophic effects on the surrounding interstellar medium (ISM). There are two main categorizations of SNe: type Ia (SNe Ia) and core-collapse (CC SNe).

SNe Ia are the thermonuclear explosions of white dwarfs, which are the leftover carbon/oxygen cores after a low-mass star (i.e. $1\ M_{\odot} \lesssim M_{\star} \lesssim 8\ M_{\odot}$) dies. One model for this ignition involves a white dwarf accreting material off a more massive companion star (the single-degenerate scenario). The second model involves the merger of two white dwarfs in a binary system (the double-degenerate scenario).

The progenitors of CC SNe are high-mass stars (i.e. $8\ M_{\odot} \lesssim M_{\star} \lesssim 30\ M_{\odot}$). There are two main types of CC SNe: type II (SNe II) and type Ibc (SNe Ibc, which is a combination of types Ib and Ic). As a high-mass star evolves, its core fuses elements into even heavier elements until it reaches iron. Eventually, nuclear fusion is unable to counteract the gravity of the star, triggering gravitational collapse. This causes the star to expel its outer layers of material in a bright explosion: a CC SN. This is the exact mechanism of a SN II. SNe Ibc are also triggered by the collapse of their cores, but their progenitor stars are ones that have

had their outer envelopes stripped away by either stellar winds or accretion by a companion.

The development of all-sky surveys (e.g. ASAS-SN) has led to an explosion in SN detections in the past few decades. While we have ideas on what differentiates the aforementioned SN subtypes, fundamental questions remain on their exact progenitors and the environments in which they explode. For this thesis, I investigated the latter by characterizing the dust, stellar, and star formation (SF) properties of SN environments.

To investigate SN environments, previous works have adopted a pixel statistic approach (e.g. James and Anderson 2006; Anderson and James 2008, 2009; Kelly et al. 2008; Habergham et al. 2010, 2012; Galbany et al. 2012; Anderson et al. 2012, 2015a,b; Anderson and Soto 2013; Kangas et al. 2013; Crowther 2013; Galbany et al. 2014; Audcent-Ross et al. 2020), many of which have been summarized in the review paper presented by Anderson et al. (2015b).

Anderson et al. (2015a) tested SNe Ia distributions against multiple bands. They found that SNe Ia trace active SF (Hα) the least than any other SN type. SNe Ia also do not trace near-UV (NUV; *GALEX*) light. Instead, this study determined that SNe Ia trace the *B*-band ("blue") light of their host galaxies better than any other band. This work also found that SNe Ia trace the *R*-band ("red") light of their host galaxies, though to a lesser degree than *B*-band light. This association with *R*-band light tells us that SNe Ia appear to trace old stellar populations. However, they noted that there appears to be "deficit" of SNe Ia at the center of galaxies as traced by *R*-band light. Anderson et al. (2015a) ruled out selection effects since their distributions showed that there is no such deficit for SNe Ibc, which are dimmer than SNe Ia. They suggested that this is rather a progenitor age and/or metallicity effect.

Anderson et al. (2012) determined that Type II SNe (SNe II) do not follow Hα, which traces active star formation. This work also found that SNe II P (a sub-type of SNe II) accurately trace the NUV emission of their host galaxies, which tracks young stellar popula-

tions. Kelly et al. (2008) also concluded that SNe II track the distribution of young stars by comparing SNe II with the distribution of g-band light of their galaxies. Furthermore, Kangas et al. (2013) found SNe II are not distributed like near-infrared (IR) light (specifically K-band).

When comparing the other core-collapse SNe (CC SNe) with Hα, Anderson et al. (2012) found that Type Ib SNe (SNe Ib) do not trace active SF whereas Type Ic SNe (SNe Ic) do. Similarly, studies have shown that SNe Ibc (a combination of SNe Ib and SNe Ic) trace active SF more closely than SNe II (Crowther, 2013; Galbany et al., 2014). Additionally, Kangas et al. (2013) found that SNe Ic are distributed like K-band flux. The authors suggested, however, that this may be due to the starburst environments in their IR-bright galaxy sample. K-band acts as a SF tracer for their sample since it is dominated by red supergiants. Furthermore, Kelly et al. (2008) determined that SNe Ib and SNe Ic are more concentrated than the g-band light of their host galaxies.

Other studies have used pixel statistics to analyze the radial distributions of CC SNe with respect to the light of their host galaxies. Habergham et al. (2012) found that SNe Ibc are more radially concentrated than SNe II. This may be because SNe Ibc are more concentrated in higher metallicity parts of galaxies, which are more centrally located (Anderson and James, 2009). Anderson and James (2009) also supported the idea that CC SNe trace active SF, as they are radially distributed like Hα. However, further studies have suggested that this centralization is more prominent in samples of interacting galaxies (Habergham et al., 2010, 2012). It is also worth noting that when these studies separated SNe Ib from SNe Ic, the SNe Ic population appeared to be more centrally concentrated than the SNe Ib population. This could be the result of SNe Ic having a tendency to occur in high-metallicity, centrally-located regions of galaxies, although Habergham et al. (2010) and Habergham et al. (2012) suggested the IMF, binarity, and stellar rotation may be at play. Overall, these works found that CC SNe are more centrally concentrated in their host galaxies, with SNe Ibc dominating

these central locations more so than SNe II (Habergham et al., 2010, 2012; Anderson et al., 2015b).

I used these previous works to formulate hypotheses for my own study. I first hypothesized that CC SNe should be tightly linked to star-forming regions of galaxies as traced by a combination of UV and mid-IR light. I also hypothesized that SNe Ia should be distributed like that of the low-mass stars of their galaxies as traced by IR light.

This thesis builds and improves upon the prominent studies reviewed in Anderson et al. (2015b) in a number of ways. First, I accumulated a more complete sample of SNe by cross-matching The Open Supernova Catalog (Guillochon et al. 2017) with a complete atlas of local ($z \sim 0$) galaxies (Leroy et al. 2019). This resulted in a sample of SNe that is larger than the samples in most of the works listed in Anderson et al. (2015b) with a total of 472 SNe. The exception is Kelly et al. 2008, who reported a sample size of ∼500 SNe.

Second, many of these studies heavily favored Hα as a SF tracer. I instead used a combination of mid-IR from WISE and far-UV (FUV) from *GALEX* to construct a SF tracer, as these bands respectively trace dust and young stellar populations. This SF band more directly traces the SFR since an extinction correction is needed when using Hα.

Third, I quantified the "environments" of SNe by using images with the same physical resolution rather than fixed angular resolution. This allowed me to describe the environments of SNe in concrete physical terms (in this case, within 0.5 kpc, 1 kpc, and 2 kpc). While Anderson et al. (2015a), for instance, averaged the physical sizes of their SN environments to be ∼300 pc, they still used imaging at fixed angular resolutions. Therefore, their physical size was not exactly the same across the galaxy sample. This appears to be the case for other works reviewed in Anderson et al. (2015b).

1.1 Contributions

I began this work in 2018 under the guidance of Dr. Dyas Utomo and Dr. Adam Leroy. Significant progress was made during the Department of Astronomy's 2019 Summer Undergraduate Research Program. This work is being translated to a paper in which I will be first author. Specific contributions to this work are as follows:

The galaxy images were processed by the z0MGS collaboration. The images were then masked and interpolated by Erica Behrens (OSU, University of Virginia), and Dr. Utomo and I aided this process by debugging the code. Dr. Leroy then convolved these images to matched physical resolutions.

I coded the programs that parsed The Open Supernova Catalog and selected our SN sample (Chapter 2); cross-matched that sample with the galaxy atlas (Chapter 2); constructed a SFR tracer (Chapter 2); built the host galaxy and SN distributions (Chapter 3); ran statistical tests and a Monte Carlo simulation (Chapter 4); and calculated SN rates (Chapter 5). Dr. Utomo significantly helped this process through code-debugging. The frequent meetings held by Dr. Utomo, Dr. Leroy, and myself led to the discussions and conclusions of this work. Dr. Utomo aided me in writing the first draft of our paper, which served as a draft of this thesis.

This thesis is organized as follows: First, I describe the galaxy maps and the selections made to The Open Supernova Catalog in Chapter 2. I then explain my methodology to build the cumulative distributions of each SN type in Chapter 3. I present the resulting SN distributions and analyze their statistical significance in Chapter 4. Finally, I interpret and summarize my findings in Chapter 5.

Chapter 2

Data

2.1 The Galaxy Sample

My galaxy sample stemmed from the $z = 0$ Multi-wavelength Galaxy Synthesis (z0MGS; Leroy et al. 2019). The z0MGS atlas contains resolved IR and UV maps of ∼16,000 bright ($M_B < -18$ mag), low-redshift ($d \lesssim 50$ Mpc) galaxies. These maps originated from two prominent NASA telescopes: the Wide-Field Infrared Survey Explorer (WISE; Wright et al. 2010) and the Galaxy Evolution Explorer (*GALEX*; Martin et al. 2005). These images highlight the dust and stellar properties of galaxies due to the wavelengths at which they were observed. It is worth noting that the z0MGS *GALEX* sample is smaller than the WISE sample due to the *GALEX* survey only covering ∼2/3 that of WISE.

W1 and W2 are WISE near-IR bands at 3.4 μm and 4.6 μm, respectively. They serve as tracers of the distribution of stellar mass in a galaxy. W3 (12 μm) and W4 (22 μm) are mid-IR bands capable of tracing dust. For *GALEX*, NUV (227 nm) and FUV (152 nm) are near-UV and far-UV bands that correspond to the emission from young stellar populations not obscured by dust.

Prior to cross-matching the z0MGS atlas with a catalog of SNe, I removed M31 and M33

from the galaxy sample because of their large angular size. This removal ensured that I did not falsely place SNe from background galaxies into these fields.

2.1.1 z0MGS Maps Interpolation and Convolution

The z0MGS maps are originally convolved at fixed angular resolutions (7.5 arcsec and 15 arcsec; Leroy et al. 2019). The beam size of the maps is $\sim$3 pixels wide, and because these galaxies are located at different distances, the physical resolution of the beam varies between them. This means that a pixel in one galaxy does not necessarily represent the same physical size as a pixel in another. Thus, it is difficult to quantify the environments of different types of SNe when the physical resolution of the pixels in which they are located are not consistent.

To capture the same environment size in which SNe are located, I used z0MGS maps that have been convolved to matched physical resolutions. These maps were created by the z0MGS team in the following way: First, masks were applied to the maps in order to identify and blank out foreground stars and galaxies. Second, the masked images were interpolated so that the blanked pixels were filled in with the median value of their surrounding pixels. Third, the images were convolved to the same physical resolutions of 0.5 kpc, 1 kpc, and 2 kpc. This convolution is analogous to placing each of the galaxies at the same distance so that each pixel has the same physical size (i.e. 0.5 kpc, 1 kpc, and 2 kpc).

The number of galaxies per physical resolution differs depending on distance. It is also worth noting that because W4 is only available at the coarser angular resolution of 15 arcsec, less W4 maps are able to be convolved to these physical resolutions. Therefore, the sample sizes of W4 galaxies and SNe are noticeably smaller.

2.1.2 Star Formation Rate Tracer

A driving force behind this work is the hypothesis that CC SNe are linked to star-forming regions of their host galaxies. To test this hypothesis, I constructed a band that traces the SF of galaxies by combining WISE's mid-IR band (W4) and *GALEX*'s FUV band. W4 is a known dust tracer while FUV traces young stars not obscured by dust, and the combination of the two captures the total SFR of galaxies. Guided by Leroy et al. (2019), I converted the W4 and FUV bands to SFR surface density ($\Sigma_{\rm SFR}$) in the following way:

For each SN in my sample, I measured the W4 flux ($I_{22\mu}$) at its pixel location and applied the equation

$$\frac{\Sigma_{\rm SFR}}{1 M_{\odot} yr^{-1}\ kpc^{-2}} \approx 3.24 \times 10^{-3} \left(\frac{C}{10^{-42.7}}\right) \left(\frac{I_{22\ \mu m}}{1 MJy\ sr^{-1}}\right), \tag{2.1}$$

where $C = 10^{-42.73}$. I then measured the FUV flux (I_{FUV}) at the same location and applied the equation

$$\frac{\Sigma_{\rm SFR}}{1 M_{\odot} yr^{-1} kpc^{-2}} \approx 1.04 \times 10^{-1} \left(\frac{C}{10^{-43.35}}\right) \left(\frac{I_{\rm FUV}}{1 MJy\ sr^{-1}}\right), \tag{2.2}$$

where $C = 10^{-43.35}$. The linear combination of these two values results in an estimated SFR at that location in a galaxy. Repeating this process for every SN in my sample provided a SFR tracer that SN distributions could be tested against.

2.2 The Supernova Sample

Previous studies (e.g. James and Anderson 2006; Anderson et al. 2012, 2015b) assembled their SN samples from only a handful of catalogs and past projects (e.g. The Asiago Supernova Catalogue). I garnered a more complete collection of SNe by drawing my sample from a heterogenous collection of all known SN data called The Open Supernova Catalog (OSC;

Guillochon et al. 2017). For each catalog entry, I made use of the following columns: Name, Disc. Date, Host Name, R.A., Dec., Type, and z. The OSC contained ∼68,000 entries at the time of this work.

2.2.1 Selections to The Open Supernova Catalog

While at the expense of excluding genuine SNe, I aimed to minimize false positives in my SN sample to ensure that this project was only working with confirmed SN events. To do so, I applied the following criteria to the OSC in order to select my sample of SNe:

1. **Discovery date.** I removed SN remnants (SNRs) by excluding OSC entries without a discovery date.

2. **Supernova types.** I removed all other entries that are not confirmed SN events. Many of these entries are not given a type (i.e. they are blank under the column "Type"), are SN candidates, are ambiguous (e.g. "Ia?"), or are not actually SNe (e.g. "Galaxy"). Thus, I only kept entries designated as SNe Ia, SNe II, SNe II P, SNe IIb, SNe II L, SNe Ib, SNe Ic, and SNe Ibc. I added SNe II P, SNe IIb, and SNe II L under the label SNe II. I also grouped SNe Ib, SNe Ic, and SNe Ibc together as SNe Ibc.

3. **Right ascension and declination.** I used recorded right ascension (RA) and declination (Dec) values in the OSC as SN locations in their host galaxies. I thus removed all OSC entries that were missing these data. For those with multiple values of RA and Dec, I took the median of each coordinate. Values of 0 were dropped for the RA before taking the median, which occurred when the RA was unknown.

These selection criteria resulted in a new version of the OSC that I deemed a "clean" cataloge, which contained 18,672 SNe.

2.2.2 Cross-matching with the *z*0MGS Maps

I further selected my sample of SNe by cross-matching this "clean" catalog with the *z*0MGS atlas. I chose to cross-match with the original atlas at fixed angular resolutions because not all galaxies were able to be convolved to physical resolutions ≤ 2 kpc. This allowed me to capture the most amount of SNe before constraining the sample.

Cross-matching involved the placement of the median RA and Dec of each SN in the W1 map of its host galaxy. I used the W1 maps because there are W1 images for all *z*0MGS galaxies. I then recorded the pixel in which the SN is located. Figure 2.1 is an example of placing SNe in the 7.5 arcsec W1 maps of their host galaxies.

This method of cross-matching did not exclude SNe that are found in blank fields nor distinguish between fields containing multiple hosts (i.e. interacting galaxies). I used the following methods in order to confirm the true host galaxy of all SNe, which involved removing SNe whose host galaxy could not be confirmed:

1. **Checking galactocentric radius.** In order to assign SNe to a galaxy, I determined that their positions must fall within a radius of 2 r_{25}. First, for each galaxy in my sample, I gathered position angles, inclinations, and optical radii (r_{25}) as recorded in the Lyon-Meudon Extragalactic Database (LEDA; Makarov et al. 2014). Second, I built an ellipse with a major axis of 2 r_{25} centered on the galaxy. I then recorded every SN that fell inside that ellipse. I only included SNe inside host galaxies with inclinations $i \leq 60^\circ$ because these galaxies are more edge-on than face-on. When a position angle or inclination was unknown, I excluded that galaxy and its SNe from my sample.

2. **Cross-matching based on host name.** Using LEDA, I matched PGC numbers to SNe that were found in *z*0MGS maps that contained more than one galaxy. This required the SNe to have recorded host names that were recognizable by LEDA. I then

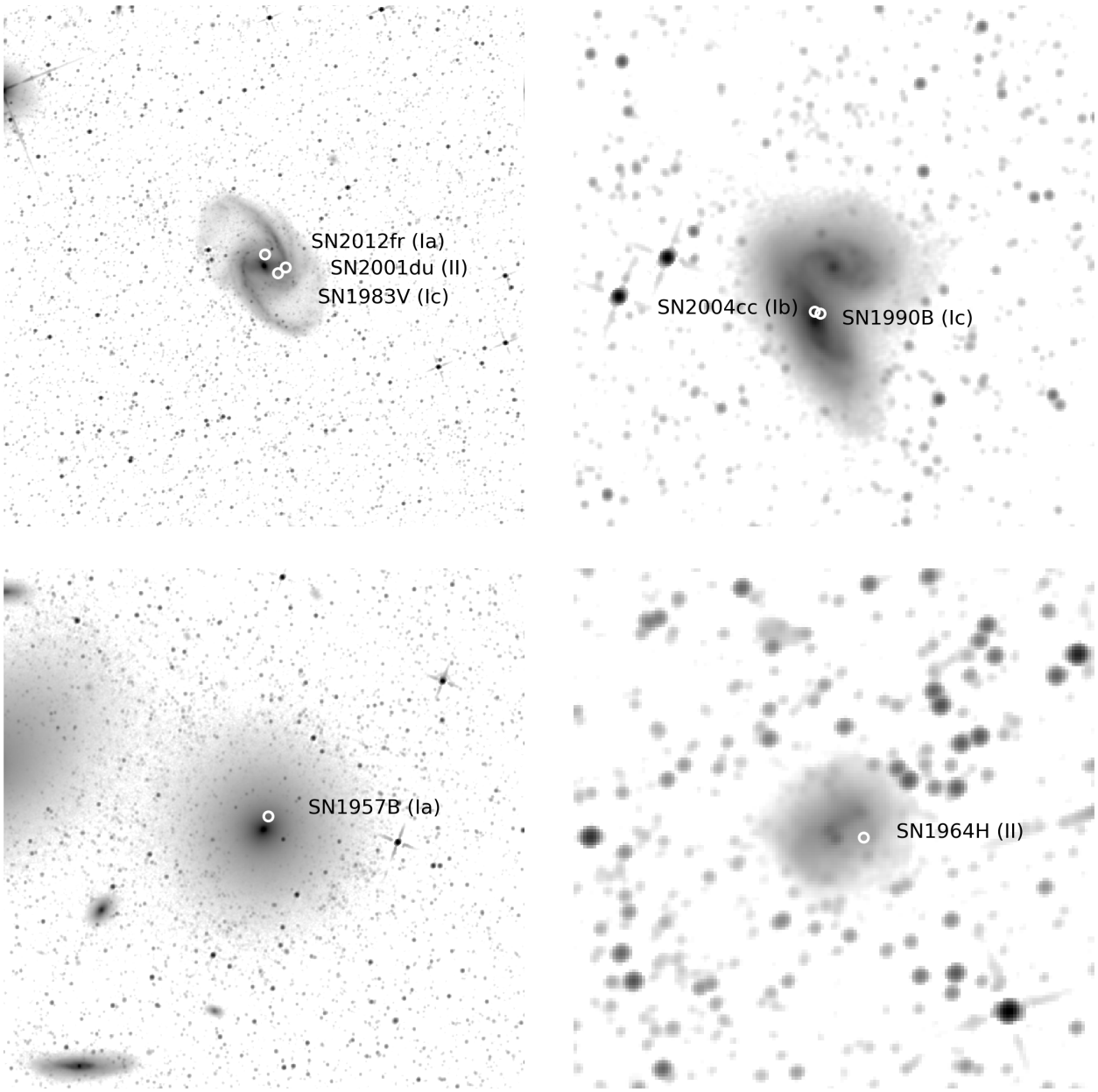

Figure 2.1 SN locations in W1 maps (7.5 arcsec resolution): NGC 1365 (PGC 13179, top left); NGC4568 (PGC 42064, top right); NGC 4374 (PGC 40455, bottom left); and NGC 7292 (PGC 68941, bottom right). SN locations are marked with a white circle, and each SN's name and type are listed.

cross-referenced each SN host's PGC number with the PGC numbers of the galaxies that were found in the same field. This allowed me to determine in which galaxy the SN truly belonged.

3. **Checking by eye.** I analyzed the W1 maps for SNe that are located inside 2 r_{25} of more than one galaxy (e.g. galaxy groups or interacting galaxies). These SNe might have also been assigned host names that are unrecognizable by LEDA. I also cross-matched the host names and PGC numbers of these SNe with the host names and PGC numbers of the galaxies that appeared in the same fields.

4. **Checking redshift.** It could be possible for SNe from background galaxies to fall within 2 r_{25} of a foreground galaxy. To ensure that no SNe in my sample were from background galaxies, I compared the SNe's recorded redshifts (z) with the redshifts of their host galaxies, which were calculated using LEDA recession velocities. If multiple redshifts were recorded for one SN, I took the median. I determined that a SN is truly within its galaxy when the difference between the galaxy's redshift and the SN's redshift is $\Delta z \lesssim 0.002$. For reference, this Δz corresponds to the ΔV of 600 km s^{-1}, which falls within the rotational velocity of a spiral galaxy.

I applied another selection criterion to ensure that my sample was not contaminated by ambiguous entries from the OSC. I flagged and excluded SNe without a recorded host name *and* redshift since they could not be verified using two of the methods listed prior. Only 12 SNe were missing these data. This resulted in 668 total SNe that could be used in my analysis. It is worth noting that more SNe are excluded from the final sample depending on the physical resolution used since not all z0MGS galaxies could be convolved to physical resolutions ≤ 2 kpc.

Table 1 is the product of these many constraints. It outlines the number of SNe per type, per band, and per resolution. I chose to work with the 2 kpc sample since this resolution is

Table 1. Final number of SNe per SN type, band, and physical resolution in my complete sample.

		Total per SN type			Total per band		
		0.5 kpc	1 kpc	2 kpc	0.5 kpc	1 kpc	2 kpc
W1	SNe Ia	11	62	142	60	218	472
	SNe II	39	115	243			
	SNe Ibc	10	41	87			
W2	SNe Ia	11	62	142	60	218	472
	SNe II	39	115	243			
	SNe Ibc	10	41	87			
W3	SNe Ia	11	62	142	60	218	472
	SNe II	39	115	243			
	SNe Ibc	10	41	87			
W4	SNe Ia	1	10	42	16	55	159
	SNe II	14	37	84			
	SNe Ibc	1	8	33			
NUV	SNe Ia	8	49	122	54	190	412
	SNe II	36	104	213			
	SNe Ibc	10	37	77			
FUV	SNe Ia	7	40	83	52	153	277
	SNe II	36	82	142			
	SNe Ibc	9	31	52			
SFR	SNe Ia	1	7	35	16	50	140
	SNe II	14	35	76			
	SNe Ibc	1	8	29			

small enough to capture localities and provided a larger sample of SNe than the 0.5 kpc and 1 kpc resolution maps. For comparison, I carried out this analysis for the 0.5 kpc and 1 kpc samples in Appendix A.1.

Chapter 3

Method

This project aimed to test the hypothesis that CC SNe (SNe II and SNe Ibc) are more concentrated in star-forming regions of their host galaxies, which UV and mid-IR (W3, W4) capture. Likewise, near-IR (W1, W2) emission traces the total distribution of stars in a galaxy. It is expected for SNe Ia to be less confined to particular regions of their hosts. Therefore, I also aimed to see how well SNe Ia trace near-IR light. In this chapter, I describe the methodology behind testing these hypotheses.

In order to compare the distributions of SN types with the UV and IR light of their galaxies, I adopted the normalized cumulative rank pixel function (NCR; James and Anderson 2006; Anderson et al. 2012, 2015b). In short, the NCR pixel statistic first involves building a cumulative distribution function (CDF) of flux (sorted by galactocentric radius) for each host galaxy (Section 3.1). This distribution represents the fraction of host galaxy flux as a function of radius from the galactic center. I next recorded the CDF value at the radius of each SN site. I finally built a cumulative distribution of those CDF values for each SN type (Section 3.2). The NCR method is further detailed in the next section (Section 3.1).

3.1 Cumulative Distributions of Host Galaxy Emission

Using the NCR pixel statistic, I applied the following steps per host galaxy:

1. **Record host galaxy flux values.** I measured the flux of each pixel inside 2 r_{25} of the host galaxy. I also set all negative emission, or noise fluctuation, to zero.

2. **Normalize and sort flux by galactocentric radius.** I normalized the flux values with respect to that of the entire host galaxy. In this case, a value of 1 indicates that a pixel has the highest emission value in the galaxy. I then sorted these normalized flux values by galactocentric radius from 0 to 2 r_{25}.

3. **Build a cumulative distribution function (CDF).** I built a CDF from these normalized and sorted flux values. Figure 3.1 illustrates this step for NGC 1365 (shown in Figure 2.1) using its 2 kpc resolution map. The x-axis is galactocentric radius and the y-axis is the cumulative fraction of flux. This CDF shows how IR and UV emission are distributed radially in the galaxy within 2 r_{25}.

I repeated these steps for every galaxy's WISE, *GALEX*, and SFR map in my sample.

3.2 Cumulative Distributions of Supernovae

To build the CDFs per SN type, I used the host galaxy CDFs constructed in Section 3.1. For each WISE, *GALEX*, and SFR map, I measured the galactocentric radius at a SN site. I interpolated its host galaxy CDF to record the CDF value at that radius (see Figure 3.1 for an illustration). This CDF value represents the fraction of total host galaxy flux within that distance from the galactic center. I repeated this process for all SNe, collecting CDF values per SN type. I then sorted these CDF values from lowest to highest and built the

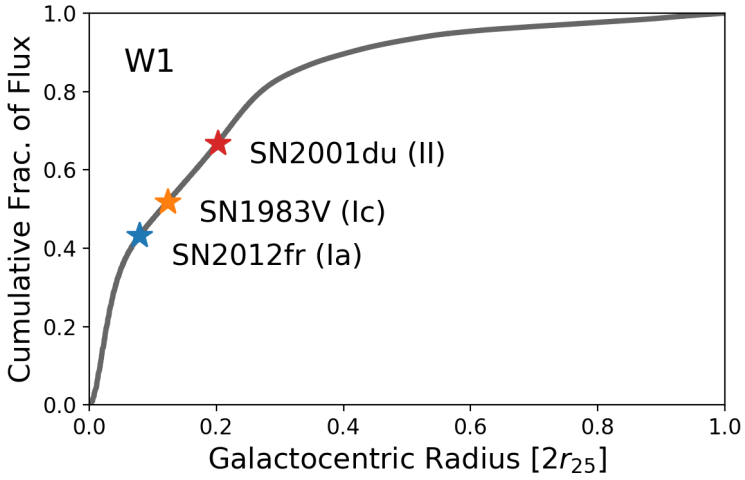

Figure 3.1 The cumulative distribution function (CDF) of W1 flux in NGC 1365 (PGC 13179) out to 2 r_{25}. This distribution records the fraction of total W1 flux inside a given radius. The galaxy CDF is normalized so that the total flux inside 2 r_{25} is unity. The star symbols mark the location (in radius) of the SNe in this galaxy. To get the CDF value of the SNe, I interpolated the host galaxy CDFs at the radius of the SNe. I repeated this process for each SN type in each band to build the CDFs of SNe.

cumulative distribution of those values. This resulted in SN CDFs, which show how well SNe of a particular type track the flux of their host galaxies.

Chapter 4

Results

Figure 4.1 shows the distributions of SNe Ia (blue), SNe II (red), and SNe Ibc (orange) using the 2 kpc resolution maps. These are the cumulative distributions of the fraction of flux within the galactocentric radius of SN sites. This fraction of flux is normalized so that the total flux within 2 r_{25} is unity. The dashed diagonal line is the expected distribution of host galaxy emission. In other words, if one were to randomly sample pixels within host galaxies, weighted by the flux of those pixels, the output would be that dashed diagonal line. In addition, I also plotted distributions of each SN type with respect to the SFR band (traced by FUV+W4) in Figure 4.2.

These SN distributions show how well each SN type follows near-IR emission (W1 and W2), mid-IR emission (W3 and W4 bands), UV emission (NUV and FUV), and the SFR of their host galaxies. If a SN population is distributed following the emission of its host galaxies, then its CDF will trace a diagonal line. If a distribution lies above this line, then that SN population tends to be more radially concentrated than its host galaxy emission. In contrast, a distribution that lies below this line indicates that this SN population tends to be more radially extended than its host galaxy emission.

In general, SNe Ibc show the most distinct distributions than the distributions of other

SNe. The distributions of SNe Ibc also have the largest separation with respect to the diagonal line. This separation is most prominent in the W4 and UV bands, which together trace the SFR. In all bands, Type Ibc distributions are more concentrated than the galaxy emission.

The distributions of SNe Ia and SNe II somewhat follow one another in the IR bands, though a small statistical difference between the two will be seen in Section 4.1. Both distributions are also more extended than the galaxy emission in the W1 and W2 bands. This is an interesting result because I hypothesized that SNe Ia would follow the stellar mass distribution, which is traced by W1 and W2. The next two sections analyze the statistical significance of my results.

4.1 Statistical Tests

A popular way to understand the similarity between two distributions is via the Kolmogorov-Smirnov (KS) test. The null hypothesis of the KS test states that two distributions are the same. When testing a given SN distribution against its host galaxy emission, the null hypothesis states that the SN distribution is the same as the host galaxy emission distribution.

The KS test outputs a statistic value, D, and a $p-$value. D measures the absolute maximum difference between two empirical cumulative distributions. Small D means both distributions are similar to each other. The $p-$value is the probability that one *cannot* reject that null hypothesis. Thus, small D also coincides with a large $p-$value.

One can *reject* the null hypothesis if D is larger than a threshold value, or rather, when the $p-$value is smaller than a given threshold α. For a one-tail test, the threshold for the $p-$value is typically $\alpha = 5\%$, which corresponds to two standard deviations away from the mean of a distribution (i.e. the 5% tail of the distribution).

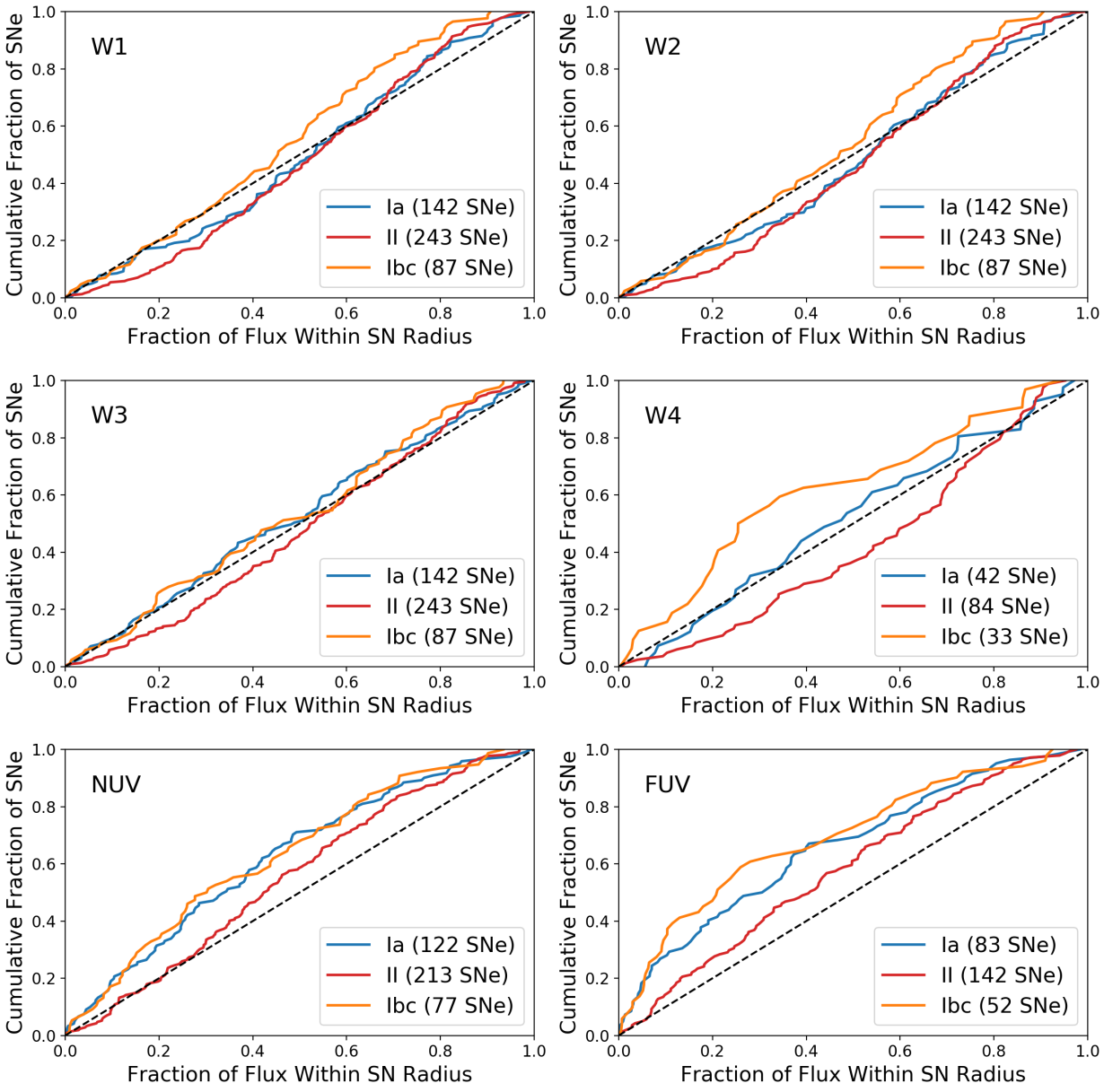

Figure 4.1 Cumulative distributions of SNe Ia (blue), SNe II (red), and SNe Ibc (orange) against host galaxy IR (W1, W2, W3, and W4), NUV, and FUV emission within 2 kpc of each SN site. The dashed diagonal line represents a uniform distribution that traces the IR and UV light of the host galaxies. If a distribution falls above the diagonal line, then that SN type tends to be more radially concentrated than host galaxy emission. If a SN population tends to be more radially extended than its host galaxy emission, then its distribution will fall below the diagonal line. The total sample of SNe is 472 for W1, W2, and W3; 159 for W4; 412 for NUV; and 277 for FUV.

Table 2. KS test results between each SN distribution and host galaxy emission (represented by the dashed, diagonal line in Figures 4.1 and 4.2) for the 2 kpc maps. To reject the null hypothesis, the statistic (D) value must be greater than a given threshold, α. The $p-$value is the probability that the null hypothesis cannot be rejected.

		$p-$value	stat. (D)	threshold	null hyp.
W1	SNe Ia	0.199	0.09	0.115	cannot reject
	SNe II	0.004	0.113	0.088	reject
	SNe Ibc	0.041	0.148	0.146	reject
W2	SNe Ia	0.121	0.099	0.115	cannot reject
	SNe II	0.003	0.117	0.088	reject
	SNe Ibc	0.055	0.143	0.146	cannot reject
W3	SNe Ia	0.479	0.07	0.115	cannot reject
	SNe II	0.03	0.093	0.088	reject
	SNe Ibc	0.407	0.094	0.146	cannot reject
W4	SNe Ia	0.91	0.085	0.21	cannot reject
	SNe II	0.049	0.147	0.149	cannot reject
	SNe Ibc	0.017	0.263	0.237	reject
NUV	SNe Ia	1.3e-05	0.22	0.124	reject
	SNe II	0.002	0.128	0.094	reject
	SNe Ibc	0.001	0.217	0.155	reject
FUV	SNe Ia	9.5e-06	0.269	0.15	reject
	SNe II	0.008	0.139	0.115	reject
	SNe Ibc	1.1e-05	0.336	0.189	reject
SFR	SNe Ia	0.194	0.179	0.23	cannot reject
	SNe II	0.142	0.101	0.13	cannot reject
	SNe Ibc	0.005	0.315	0.253	reject

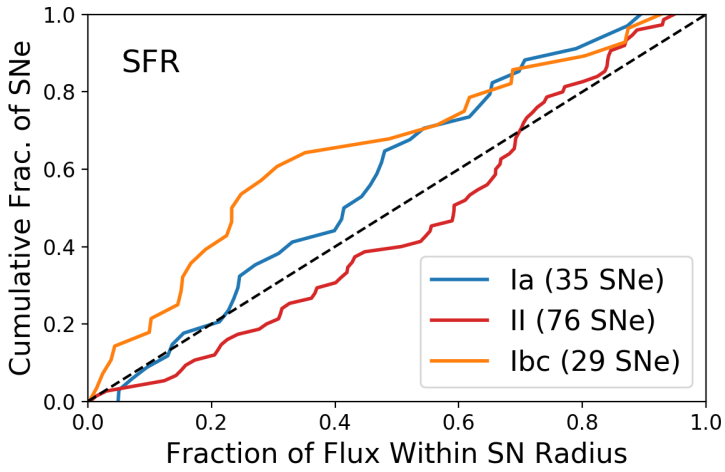

Figure 4.2 Cumulative distributions of SNe Ia (blue), SNe II (red), and SNe Ibc (orange) against the SFR tracer, which is a combination of W4 and FUV light, for the 2 kpc maps. The dashed diagonal line represents a uniform distribution that traces the IR and UV light of the host galaxies. If a distribution falls above the diagonal line, then that SN type tends to be more radially concentrated than host galaxy emission. If a SN population tends to be more radially extended than its host galaxy emission, then its distribution will fall below the diagonal line. The total sample of SNe is 140.

Equivalently, one can *reject* the null hypothesis at a level of $\alpha = 5\%$ when

$$D > c(\alpha) \left(\frac{m+n}{m \times n} \right)^{0.5}, \tag{4.1}$$

where $c(\alpha) = c(0.05) = 1.385$ and m and n are the sample sizes of the two distributions.

I performed the KS test between all SN distributions and their host galaxy emission distributions. The results (i.e. the statistic value D, the $p-$value, and the threshold value) are listed in Table 2.

SNe Ia trace W4 light to a highly significant degree with a $p-$value of 91%. In general, SNe Ia have a higher degree of association with W1, W2, and W4 light than SNe II and SNe Ibc. The null hypothesis could not be rejected for SNe Ia in all bands except NUV and FUV.

SNe II have the highest degrees of association with the SFR tracer ($p-$value = 14.2%)

and W4 ($p-$value = 4.9%). While the KS test rejects the hypothesis that the W3 and SNe II distributions are same, the threshold and D values are relatively close.

SNe Ibc have the weakest association to their host galaxy emission for all UV and IR bands. The null hypothesis is rejected for SNe Ibc in every band except W2 and W3. However, the degrees of association are weaker, with a $p-$value of only 5.5% for W2 and 1.7% for W3. Additionally, the threshold and D value for SNe Ibc in W1 are extremely close (0.146 and 0.148, respectively). The lowest $p-$values recorded in Table 2 are SNe Ia in NUV and FUV (1.3×10^{-5} and 9.5×10^{-6}, respectively) and SNe Ibc in FUV (1.1×10^{-5}). This can be visually seen in Figure 4.1, where the orange SNe Ibc distributions are pulled far up and to the left for NUV and FUV.

4.2 Monte Carlo Simulations

The effect of sample size is not readily captured in the KS test. To assess the uncertainty brought about by a limited sample size, I constructed a Monte Carlo simulation.

I first randomly selected a pixel in each band (weighted by the flux itself) and built a CDF with the same method used to build the SN distributions (see Chapter 3). I limited the sample to be equal to each SN type's sample. I then repeated this process 100 times to get 100 distributions. The variation of these distributions illustrates the uncertainty of the CDF in each band.

Figure 4.3 shows the SNe Ia, SNe II, and SNe Ibc distributions (i.e. the red, blue, and orange curves) with respect to 100 simulated CDFs per band (i.e. the gray curves). Results show that SNe Ia are within the variance of the WISE bands and SFR tracer, which is supported by the KS test results. The SNe Ia distributions fall outside the uncertainty of the UV bands, supporting the KS test result that the null hypothesis is rejected for SNe Ia in UV.

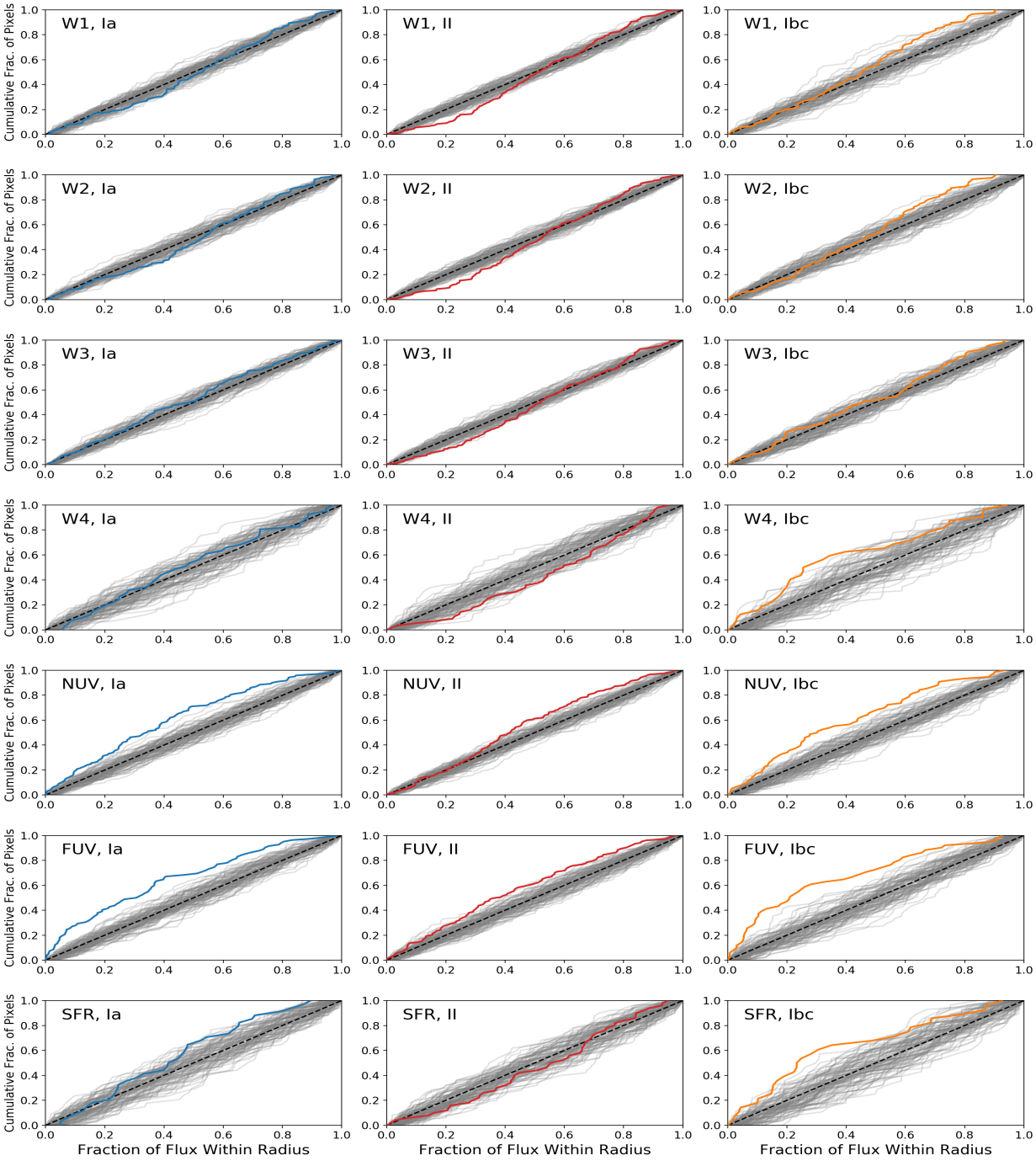

Figure 4.3 For each band, I ran a Monte Carlo simulation to test the uncertainty of each SN distribution. I first selected a random sample n pixels, where n is the number of SNe in that particular sample. For instance, when running the Monte Carlo simulation for SNe Ia in W1, I limited the sample to 142 pixels because the SNe Ia sample is 142 in W1. I built the simulated CDFs the same way I constructed the SN CDFs in Section 3.2. The gray distributions are the product of running the simulation 100 times per band, per SN type. I overlaid the actual SN CDF atop the simulated distributions to see if the SN CDF lies within the spread of possible distributions.

The KS test rejected the null hypothesis that SNe II and the W1, W2, and W3 bands are distributed the same. The Monte Carlo simulation results agree with that at low galactocentric radii. It appears that SNe II are more extended than the more centrally-concentrated light of their host galaxies in these bands. It is worth noting that the SNe II distribution in W3 is very close to boundaries of the variance, as supported by the close D and threshold values.

The null hypothesis for SNe II is not rejected for W4 or the SFR tracer. The Monte Carlo simulation shows that the distributions lie within the variance of these bands, though this could be an effect of small sample size. I also note that while the KS test states that SNe II are not distributed like the UV light of their galaxies, SNe II have a closer association with this type of light than SNe Ia and SNe Ibc. The SNe II distribution is also within the uncertainty at lower galactocentric radii.

Small sample size comes into play with SNe Ibc in W4. The KS test rejects the hypothesis that these two distributions are the same. The Monte Carlo simulation, however, shows that the W4 uncertainty is quite wide. The KS test draws the same conclusions for SNe Ibc in W1, though the Monte Carlo test shows that the SNe Ibc distribution lies within the expected uncertainty until very high radii.

In summary, the Monte Carlo simulation provides a look at the uncertainty of the distributions. It supports the rejection of the null hypothesis for SNe Ia in UV, SNe II in W1, W2, W3, and UV, and SNe Ibc in W1, W4, UV, and the SFR band. It also shows that at some radii, the SN distributions lie within the uncertainty of these bands, indicating that some SN types might follow the IR or UV light of their host galaxies at only certain galactocentric radii.

Chapter 5

Discussion & Conclusions

I had hypothesized that SNe Ia would have the highest degree of association with W1 light. W1 is considered to trace the total distribution of all stars, and because SNe Ia are the thermonuclear explosions of white dwarfs, I expected SNe Ia to be distributed like the low-mass stars of their host galaxies.

My hypothesis is consistent with the $p-$values per SN type for W1 light (Table 2). SNe Ia trace the W1 light of their host galaxies to a higher degree than SNe II and SNe Ibc. I also found that SNe Ia trace W4 to a higher degree than W1. A partial reason for this is that SNe Ia do not necessarily trace W1 light, but rather the distribution of stellar mass. Stellar mass surface density depends on W1 light and a mass-to-light ratio. This means that SNe Ia may in fact be distributed like that of stellar mass if I were to apply a mass-to-light ratio correction to W1.

SNe Ia are not distributed like the UV light of their host galaxies, as supported by both the KS test and the Monte Carlo simulations. On the other hand, SNe Ia do appear to somewhat trace the SFR, which is due to SNe Ia's close association with W4 light.

I had also hypothesized that CC SNe would have the highest degree of association with dust tracers (W3 and W4), young stars (NUV and FUV), and the SFR tracer. This is

because CC SNe are expected to be tightly linked to regions of active SF and dust in their host galaxies.

SNe II do not appear to trace the dust of their host galaxies. The $p-$value for W4 (4.9%) suggests that SNe II do not trace this band, though this value is *just* under 5%. The $p-$value for W3 (3%) and the Monte Carlo simulation both agree with the rejection of the null hypothesis for SNe II in W3.

SNe II also do not appear to trace young stars. The $p-$values for SNe II in the UV bands are low enough for the null hypothesis to be rejected. The Monte Carlo simulation supports this at higher radii but also shows that the distributions are within the expected uncertainty at lower galactocentric radii. This low association between UV light and SNe II may be due to UV light being blocked by dust at the center of galaxies. This causes the distribution of UV light to be more extended, resulting in the SNe II population appearing to be more concentrated than UV light. This would explain why all SN populations appear more radially concentrated than NUV and FUV light.

SNe II have the highest $p-$value with the SFR tracer (14.2%). This suggests that these types of SNe trace active SF to a fairly significant degree.

Results for SNe Ibc are puzzling due to low $p-$values. I expected SNe Ibc to be tied to regions of young stars and active SF. However, I found that SNe Ibc are not distributed like the NUV, FUV, or SFR bands. SNe Ibc have weaker associations with these bands than W1, W2, and W3. The $p-$values for W1 and W2 are small at 4.1% and 5.5%. The association with W3 is much higher at 40.7%, and so SNe Ibc appear to be linked to regions of dust. It is possible that SNe Ibc do not show the same degree of association with W4 light due to a smaller sample size in this band. This explanation is further supported with the somewhat close threshold and D value (0.237 and 0.263, respectively) and the uncertainty assessed by the Monte Carlo simulation.

5.1 Supernova Rate in Nearby Galaxies

I took advantage of the large number of SNe (472) and galaxies (359) included in this study and estimated the rate of SNe (the number of SNe per century) in nearby galaxies ($d < 50$ Mpc). There are multiple ways to derive the SN rate: 1.) SN rate per stellar mass of nearby galaxies; 2.) SN rate per SFR of nearby galaxies; and 3.) SN rate per galaxy morphology.

There are two limitations to these calculations. First, the z0MGS sample is only complete for galaxies with distance $d < 50$ Mpc and brightness of $M_B < -18$ mag. Second, the OSC does not capture all SNe in the local volume. The SN rate has also emerged recently in the last decade due to all-sky surveys with high cadence (e.g. ASAS-SN). Therefore, the results are presented with high and low estimates using the following methods: First, I included the entire z0MGS sample. This results in the lower limit of the SN rate. Second, I only included the host galaxies of SNe, resulting in the upper limit of the SN rate. The true SN rate lies between these upper and lower limits. For both of these limits, I only included SNe discovered between the years 2000 and 2020 since their rate of discovery was more consistent between these years.

For this calculation, I did not limit the sample based on type so long as each SN was designated one (e.g. I kept SNe Ia-Pec, SNe IIn, SNe Ic Pec, SNe Ic BL, etc). I added these sub-types to their general categories (e.g. SNe IIn are now under SNe II), except for "peculiar" SNe and SNe Ic BL, which I only included in the calculations for all SNe. Similarly, I only included SNe with uncertain type assignments (e.g. "Ib/IIb") in the calculations for all SNe. Candidates were completely excluded due to the possibility of not being SNe at all.

Additionally, I chose to use the z0MGS atlas at fixed angular resolution to include galaxies that could not be convolved to a physical resolution of ≤ 2 kpc. However, I limited the sample to only include galaxies within d ≤ 50 Mpc for completeness. I also only included galaxies

Table 3. SN rate per unit stellar mass defined by the number of SNe per 100 years per $10^{10} M_{\odot}$. I analyzed these SN rates with respect to SN type, galaxy morphology, and galaxy stellar mass. The lower limit is using all galaxies in the z0MGS sample with $d < 50$ Mpc and $i < 60$. The upper limit is using only SN host galaxies with $d < 50$ Mpc and $i < 60$.

Selections	SNe Ia	SNe II	SNe Ibc	All SNe
None	0.086−1.41	0.176−2.762	0.069−2.97	0.347−2.25
$T < -2$	0.058−0.85	0.01−1.53	0.003−1.17	0.08−0.915
$-2 < T < 0$	0.049−1.43	0.01−0.998	0.01−16.18	0.08−1.23
$0 < T < 2$	0.095−2.03	0.074−3.66	0.032−1.55	0.212−2.16
$2 < T < 4$	0.126−1.27	0.23−1.622	0.12−2.64	0.507−1.749
$4 < T < 6$	0.099−2.71	0.611−4.39	0.225−3.29	0.971−3.87
$6 < T < 8$	0.121−19.21	0.523−7.43	0.121−28.3	0.805−9.48
$8 < T < 10$	0.134−32.8	0.47−2.78	0.067− ⋯	0.872−5.011
$10^{9} M_{\odot} < M_{\star} < 10^{9.5} M_{\odot}$	0.221−25.11	0.478−27.99	0.184−21.07	0.919−25.9
$10^{9.5} M_{\odot} < M_{\star} < 10^{10} M_{\odot}$	0.15−8.56	0.414−9.765	0.1−8.21	0.689−9.25
$10^{10} M_{\odot} < M_{\star} < 10^{10.5} M_{\odot}$	0.117−2.82	0.268−3.8	0.127−3.268	0.545−3.36
$10^{10.5} M_{\odot} < M_{\star} < 10^{11} M_{\odot}$	0.065−1.033	0.112−1.28	0.046−1.55	0.242−1.24
$M_{\star} > 10^{11} M_{\odot}$	0.041−0.387	0.02−0.766	0.005− ⋯	0.071−0.541

with an inclination $i \leq 60°$ since detecting SNe at higher inclinations is difficult due to dust extinction. This limited the galaxy sample and SN sample to 290 and 234, respectively, for this calculation.

The estimated SN rate per stellar mass is 0.35 SNe per 100 years per 10^{10} $M_{\odot}$ when using all z0MGS galaxies with $d < 50$ Mpc and $i \leq 60°$. For the upper limit of just using host galaxies, the SN rate becomes 2.25 SNe per 100 years per 10^{10} $M_{\odot}$ (Table 3). This range is in line with what is observed in the Milky Way. There are two caveats to this calculation: First, low-mass galaxies are missing in the z0MGS sample, which would result in a lower SN rate. Second, the SN sample could also be incomplete, which would produce a higher SN rate.

I grouped the galaxies based on their morphological types. Generally, S0 and ellipticals have $T-$types ≤ 2, spirals have $2 < T < 6$, and dwarfs and irregulars have $T \geq 6$. I grouped

Table 4. SN rate per unit SFR defined by the number of SNe per 100 years per $M_\odot$ yr^{-1}. I analyzed these SN rates with respect to SN type, galaxy morphology, and galaxy stellar mass. The lower limit is using all galaxies in the $z0$MGS sample with $d < 50$ Mpc and $i < 60$. The upper limit is using only SN host galaxies with $d < 50$ Mpc and $i < 60$.

Selections	SNe Ia	SNe II	SNe Ibc	All SNe
None	0.166−3.8	0.329−1.556	0.129−2.22	0.66−2.073
$T < -2$	0.747−24.3	0.16−4.36	0.05−72.27	1.07−15.29
$-2 < T < 0$	0.172−17.34	0.034−11.99	0.034−10.69	0.276−15.84
$0 < T < 2$	0.212−6.38	0.165−1.48	0.071−6.73	0.472−2.997
$2 < T < 4$	0.173−2.2	0.32−1.34	0.159−1.5	0.701−1.636
$4 < T < 6$	0.094−2.04	0.581−3.35	0.214−2.52	0.924−2.94
$6 < T < 8$	0.147−17.35	0.638−8.56	0.147−26	0.982−10.25
$8 < T < 10$	0.03−17.21	0.11−0.221	0.015− ⋯	0.198−0.407
$10^9 M_\odot < M_\star < 10^{9.5} M_\odot$	0.146−15.31	0.379−19.326	0.146−19.88	0.7−18.57
$10^{9.5} M_\odot < M_\star < 10^{10} M_\odot$	0.141−8.43	0.386−19.33	0.094−6.3	0.645−5.4
$10^{10} M_\odot < M_\star < 10^{10.5} M_\odot$	0.155−3.41	0.387−3.273	0.183−2.27	0.774−3.02
$10^{10.5} M_\odot < M_\star < 10^{11} M_\odot$	0.174−2.41	0.298−1.018	0.124−1.23	0.645−1.38
$M_\star > 10^{11} M_\odot$	0.181−4.06	0.091−0.125	0.023− ⋯	0.317−0.413

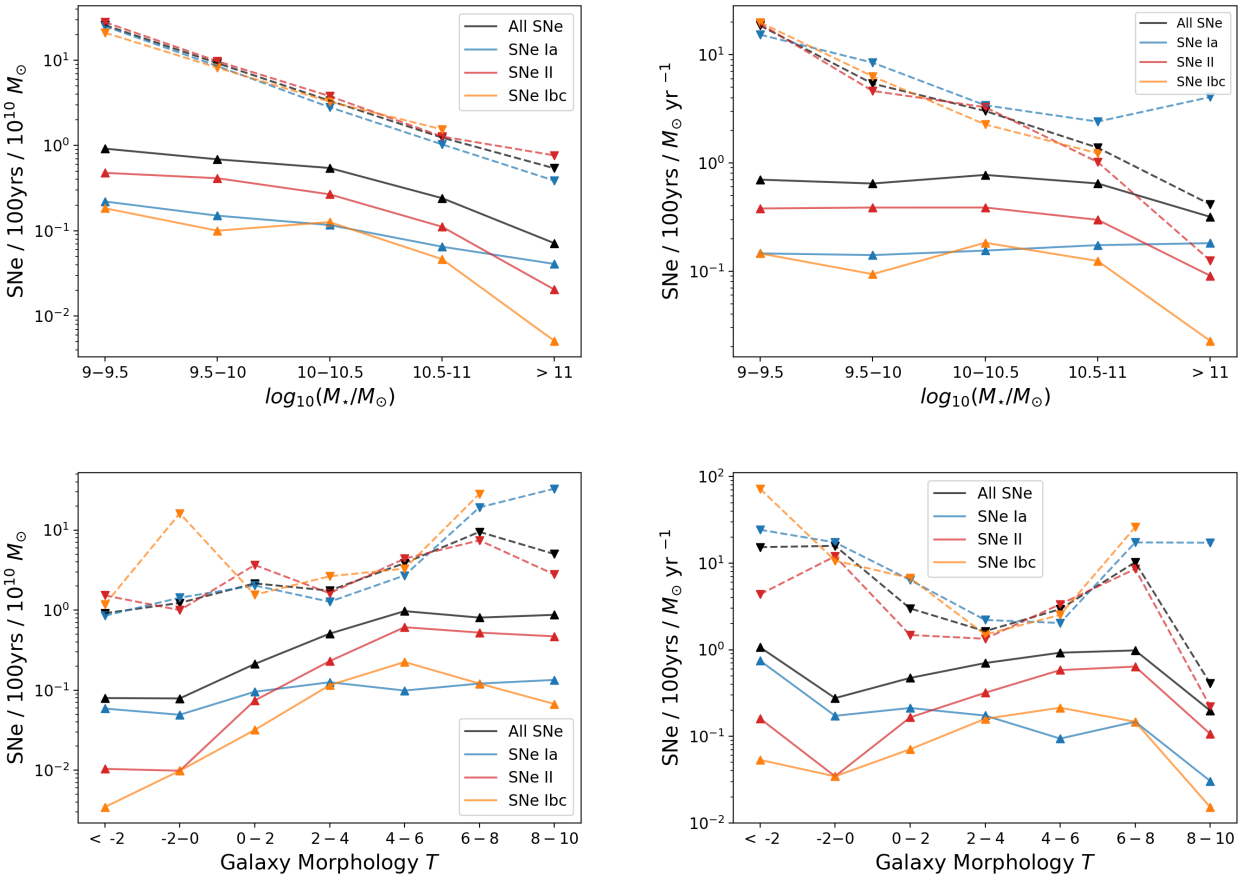

Figure 5.1 SN rates indicated by the number of SNe per 100 years per $10^{10} M_{\odot}$ (left) and per SFR (right). These rates are binned by galaxy mass (top) and morphological $T-$types (bottom). The dashed lines connecting the downward-facing triangles show the trends of the upper-limits to this calculation, which stemmed from only using host galaxies. The solid lines and upward-facing triangles illustrate the lower-limit trends, which were calculated using all $z0$MGS galaxies within $d \leq 50$ Mpc and $i \leq 60$. These trends show that the rate of SNe Ia is more consistent than other SN types in galaxies of different mass. SNe Ibc rates drop off faster than SNe II rates in galaxies with $T > 4$, supporting the idea that SNe Ibc are found in high-metallicity regions. Additionally, there appear to be higher rates of CC SNe in spirals (intermediate mass, $T-$types between 2 and 6).

these $T-$types into finer bins to reveal a trend (Table 3; Figure 5.1). The highest SN rate occurs in dwarfs and irregulars ($0.81-9.5$), followed by spirals ($0.51-3.87$). The lowest rate is found in early-type galaxies ($0.08-2.16$). This is expected because late-type galaxies are more star-forming, and so that they have a higher overall SN rate.

Additionally, I grouped the galaxies into six bins of total stellar mass with a width of 0.5 dex (Table 3). A similar trend is also observed here because low-mass galaxies tend to have high $T-$values. I found the highest SN rate in low mass galaxies ($0.92-25.9$), followed by intermediate mass galaxies ($0.55-9.3$), and high mass galaxies ($0.07-1.24$).

It is interesting to note that the SN Ia rate is lower in early-type galaxies even though SNe Ia are thought to originate from old stellar populations. Furthermore, the lower limit of the SN Ia rate is similar for both spirals and irregulars and for both low and intermediate mass galaxies. The lower limit of the SN Ia rate in early-type galaxies (0.058) is higher than the lower limit of the SN II (0.01) and SN Ibc rates (0.003). This is expected because early-types are no longer star-forming.

Figure 5.1 illustrates the SN rate trends. The lower SN Ia rate is more shallow than the other SN types across all galaxy masses. This indicates that the rate of SNe Ia is more consistent with respect to galaxy mass than SNe II and SNe Ibc. This result supports the idea that SNe Ia progenitors have longer delay times since more massive galaxies are dominated by older stellar populations.

We also find that the SN Ibc rate drops off faster around morphological type $T = 4$ than the SN II rate. Galaxies with $T-$types higher than 6 are designated as dwarfs and irregulars, which have less mass and lower metallicities. This supports the idea that SNe Ibc progenitors are tied to high-metallicity environments. It also appears that CC SNe have higher rates in spiral galaxies.

I repeated this analysis per SFR and found that the estimated SN rate lies between 0.66 and 2.07 SNe per 100 years per $M_{\odot}$ yr^{-1} (Table 4), which is also in line with the observed

rate in the Milky Way. Figure 5.1 conveys the trends of these rates per SFR, which support the stellar mass trends. Generally, the SN Ia rate is higher than the CC SN rate in early-type galaxies, whereas the total SN rate and CC SN rate are higher in spirals. As noted before, the SN Ibc rate drops off faster than the SN II rate in dwarfs and irregulars.

5.2 Summary

The key conclusions of this work are as follows:

1. SNe Ia trace the stellar distribution of their host galaxies. The Monte Carlo simulation in Chapter 4 showed that the SNe Ia distributions follow the WISE light of their host galaxies within the uncertainty estimated by the limited sample size of SNe.

2. SNe II trace the SF of their host galaxies. This supports the idea that their progenitors are high-mass, young stars.

3. SNe Ibc appear to be distributed like the dust of their host galaxies as traced by W3. This association with dust indicates that their progenitors are born in high-metallicity regions, supporting Anderson et al. (2015b). However, SNe Ibc are not distributed like W4 light, another dust tracer, though this is most likely due to a small sample size. Similarly, the SN Ibc rate drops sharply for low-metallicity galaxies.

4. The estimated SN rate for galaxies with $d < 50$ Mpc and $i \leq 60°$ is $0.4 - 2.3$ SNe per 100 years per 10^{10} $M_{\odot}$, which aligns with the observed rate in the Milky Way ($\sim$1 SN every 100 years). A similar range was calculated per SFR ($0.7 - 2.1$ SNe per 100 years per $M_{\odot}$ yr^{-1}).

Appendix A

Alternative Plots

A.1 0.5 kpc and 1 kpc Maps

To explore the SN distributions at sharper resolutions, I used z0MGS maps that were interpolated and convolved to physical resolutions of 0.5 kpc and 1 kpc. I repeated the steps in Chapter 3 to build the SN cumulative distributions for each band at these physical resolutions, resulting in Figures A.1, A.2, A.3. Tables 5 and 6 are KS test results of these distributions.

As one can see, sample size really plays a role in constructing the SN distributions. Less than 50 SNe are captured at a resolution of 0.5 kpc. In turn, there is a higher uncertainty in the KS test results at this resolution, as it is difficult to reject the null hypothesis that the SN distribution is the same as the host galaxy distribution of a particular band when dealing with only a handful of SNe.

A larger sample is captured at 1 kpc than 0.5 kpc, but still not at the level of the 2 kpc sample. Less SN distributions can be rejected at 1 kpc. However, a larger sample provides a distribution with less uncertainty, as shown in the Monte Carlo simulation in Chapter 4. This led to the decision to use 2 kpc as my working resolution.

A.2 Removing Selection Based on Inclination

In Chapter 3, I selected SNe that are located in galaxies with inclinations $i \leq 60$. Galaxies with $i > 60$ are highly inclined, and the measured flux of a pixel in a edge-on galaxy is difficult to interpret. Here, I explored the effects of including all SNe in the 0.5 kpc, 1 kpc, and 2 kpc samples regardless of host galaxy inclination (Figures A.4, A.5, and A.6). I did the same for the SFR tracer (Figure A.7).

One can visually see that the SN distributions change when including an inclination selection versus not. For example, one can compare the 2 kpc SN distributions with this inclination cut (Figure 4.1) with the 2 kpc SN distributions with no inclination cut (Figure A.6). In Figure 4.1, SNe Ia and SNe II appear to be more extended at lower galactocentric radii than what is shown in Figure A.6. Additionally, SNe II follow NUV light at lower galactocentric radii in Figure 4.1 than Figure A.6. Furthermore, the SN distributions in FUV appear to deviate more from the host galaxy distribution in Figure A.6 than Figure 4.1. These are just some examples illustrating how galaxy inclination can affect the SN distributions.

While excluding SNe in galaxies $i \geq 60$ heavily reduced my sample, I determined that the effect of galaxy inclination on the measurements was too significant to ignore. Anderson et al. (2012) make similar selections by removing all SNe in galaxies with axis ratios higher than 4:1.

A.3 Selection Based on Supernova Discovery and Galaxy Imaging Dates

Anderson et al. (2012) exclude all SNe that were discovered within 1 year of galaxy imaging for SNe Ibc and 1.5 years for SNe II. This selection is made in order to prevent measuring

any remaining SN emission post-explosion. I explored this idea by excluding all SNe that were discovered between 2003 and 2013. This selection is based on WISE and *GALEX* operations. *GALEX* operated from 2003 to early 2012, and WISE operated between those dates. I constructed the SN distributions for these sub-samples at all resolutions (Figures A.8, A.9, A.10). I did the same for the SFR tracer (Figure A.11).

I next performed a KS test between the CDFs with no selections based on SN discovery date and the new CDFs with selections based on SN discovery date for the 2 kpc sample. The KS test was taken between the same SN types per band. The resulting $p-$values are very near 100%, the smallest being 94% for SNe Ibc in the W3 band and 97% for SNe Ia in W2. All other p-values are $\sim 99\%$ or higher. Thus, I determined that there is no significant difference between excluding SNe that were discovered during WISE and *GALEX* imaging operations and keeping these SNe in the sample. I chose to keep these SNe in order to capture a larger sample.

Table 5. The result of performing a KS-test between each 0.5 kpc sample SN distribution and host galaxy emission (represented by the dashed, diagonal line in Figures A.1 and A.3). To reject the null hypothesis, the statistic (D) value must be greater than a given threshold, α. The $p-$value is the probability that the null hypothesis cannot be rejected.

		$p-$value	stat. (D)	threshold	null hyp.
W1	SNe Ia	0.712	0.202	0.41	cannot reject
	SNe II	0.245	0.161	0.218	cannot reject
	SNe Ibc	0.102	0.368	0.43	cannot reject
W2	SNe Ia	0.729	0.199	0.41	cannot reject
	SNe II	0.222	0.165	0.218	cannot reject
	SNe Ibc	0.134	0.35	0.43	cannot reject
W3	SNe Ia	0.445	0.249	0.41	cannot reject
	SNe II	0.509	0.129	0.218	cannot reject
	SNe Ibc	0.086	0.379	0.43	cannot reject
W4	SNe Ia	0.615	0.616	1.36	cannot reject
	SNe II	0.773	0.17	0.363	cannot reject
	SNe Ibc	0.374	0.743	1.36	cannot reject
NUV	SNe Ia	0.262	0.337	0.48	cannot reject
	SNe II	0.566	0.128	0.227	cannot reject
	SNe Ibc	0.084	0.38	0.43	cannot reject
FUV	SNe Ia	0.075	0.457	0.513	cannot reject
	SNe II	0.393	0.147	0.227	cannot reject
	SNe Ibc	0.03	0.46	0.453	reject
SFR	SNe Ia	0.621	0.613	1.36	cannot reject
	SNe II	0.792	0.167	0.363	cannot reject
	SNe Ibc	0.433	0.709	1.36	cannot reject

Table 6. The result of performing a KS-test between each 1 kpc sample SN distribution and host galaxy emission (represented by the dashed, diagonal line in Figures A.2 and A.3). To reject the null hypothesis, the statistic (D) value must be greater than a given threshold, α. The $p-$value is the probability that the null hypothesis cannot be rejected.

		$p-$value	stat. (D)	threshold	null hyp.
W1	SNe Ia	0.252	0.127	0.173	cannot reject
	SNe II	1.9e-04	0.199	0.127	reject
	SNe Ibc	0.028	0.224	0.213	reject
W2	SNe Ia	0.249	0.128	0.173	cannot reject
	SNe II	2.2e-04	0.198	0.127	reject
	SNe Ibc	0.111	0.184	0.213	cannot reject
W3	SNe Ia	0.989	0.056	0.173	cannot reject
	SNe II	0.019	0.142	0.127	reject
	SNe Ibc	0.064	0.201	0.213	cannot reject
W4	SNe Ia	0.271	0.301	0.43	cannot reject
	SNe II	0.35	0.15	0.224	cannot reject
	SNe Ibc	0.041	0.466	0.48	cannot reject
NUV	SNe Ia	0.098	0.172	0.194	cannot reject
	SNe II	0.488	0.081	0.134	cannot reject
	SNe Ibc	1e-04	0.358	0.224	reject
FUV	SNe Ia	0.025	0.229	0.215	reject
	SNe II	0.165	0.122	0.151	cannot reject
	SNe Ibc	2.63e-05	0.416	0.244	reject
SFR	SNe Ia	0.464	0.303	0.513	cannot reject
	SNe II	0.655	0.121	0.23	cannot reject
	SNe Ibc	0.018	0.515	0.48	reject

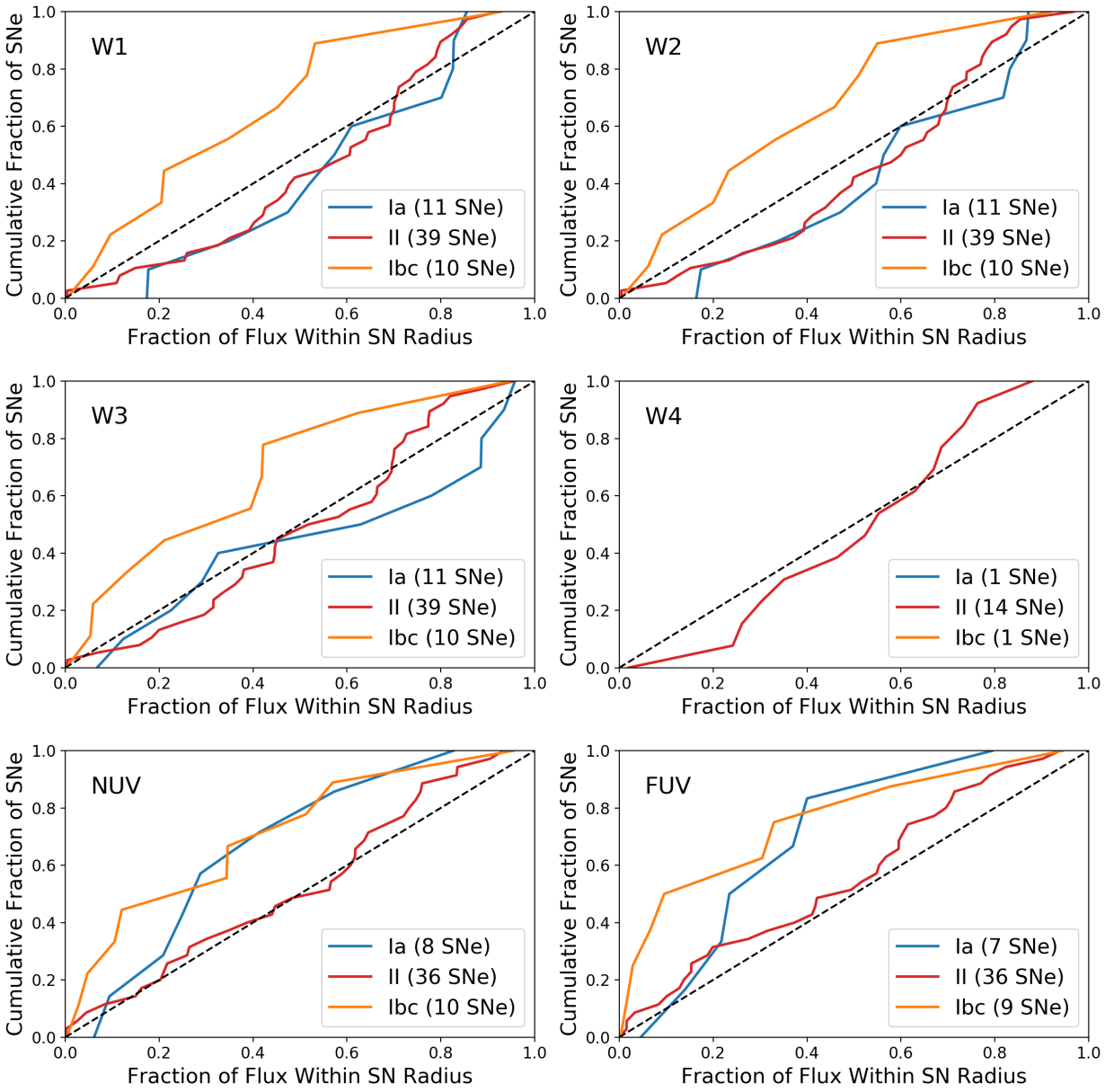

Figure A.1 Cumulative distributions of SNe Ia (blue), SNe II (red), and SNe Ibc (orange) against host galaxy IR (W1, W2, W3, and W4), NUV, and FUV emission within **0.5 kpc** of each SN site. The dashed diagonal line represents a uniform distribution that traces the IR and UV light of the host galaxies. If a distribution falls above the diagonal line, then that SN type tends to be more radially concentrated than host galaxy emission. If a SN population tends to be more radially extended than its host galaxy emission, then its distribution will fall below the diagonal line. The total sample of SNe is 60 for W1, W2, and W3; 16 for W4; 54 for NUV; and 52 for FUV.

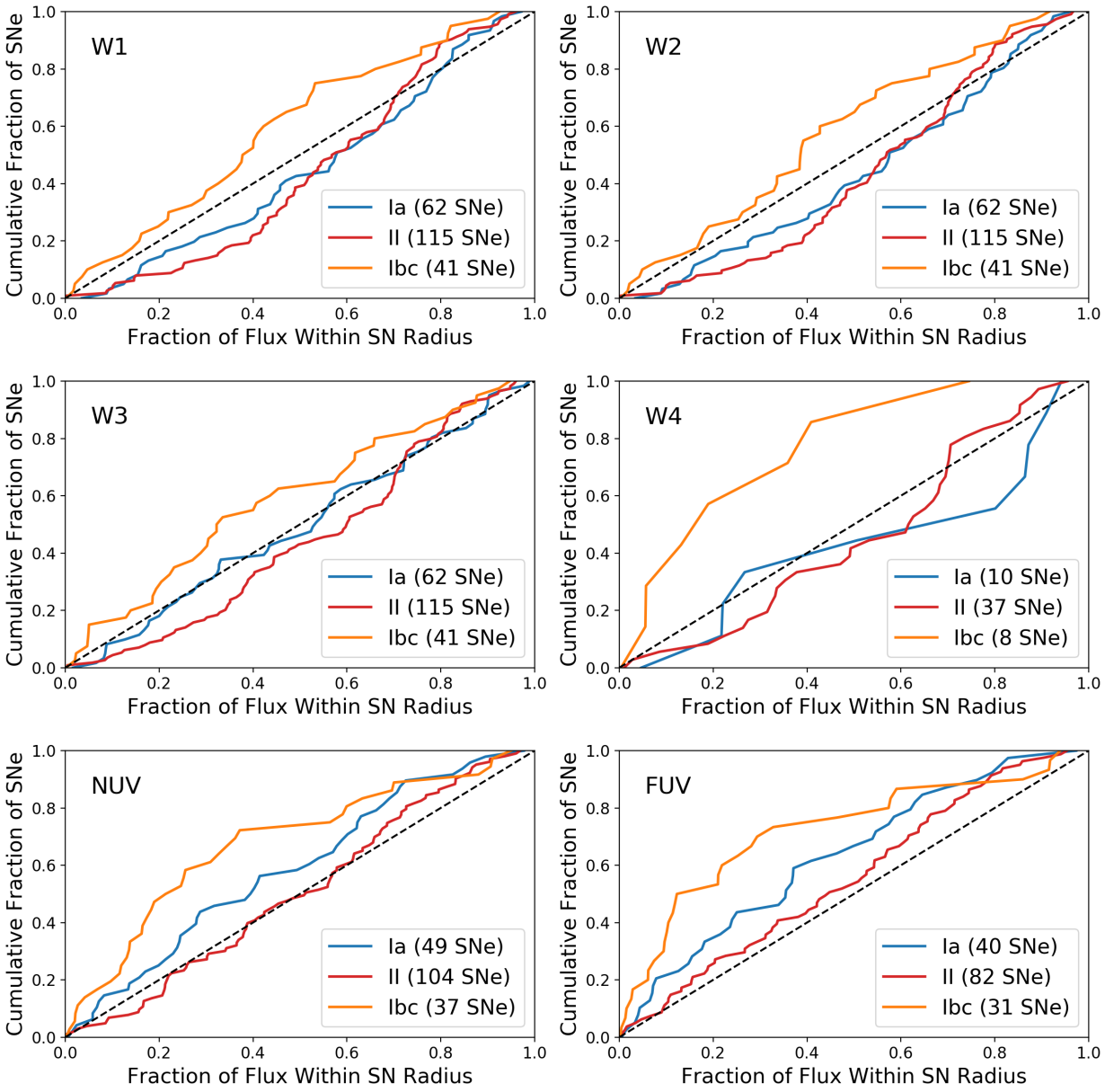

Figure A.2 Cumulative distributions of SNe Ia (blue), SNe II (red), and SNe Ibc (orange) against host galaxy IR (W1, W2, W3, and W4), NUV, and FUV emission within **1 kpc** of each SN site. The dashed diagonal line represents a uniform distribution that traces the IR and UV light of the host galaxies. If a distribution falls above the diagonal line, then that SN type tends to be more radially concentrated than host galaxy emission. If a SN population tends to be more radially extended than its host galaxy emission, then its distribution will fall below the diagonal line. The total sample of SNe is 184 for W1, W2, and W3; 43 for W4; 158 for NUV; and 126 for FUV.

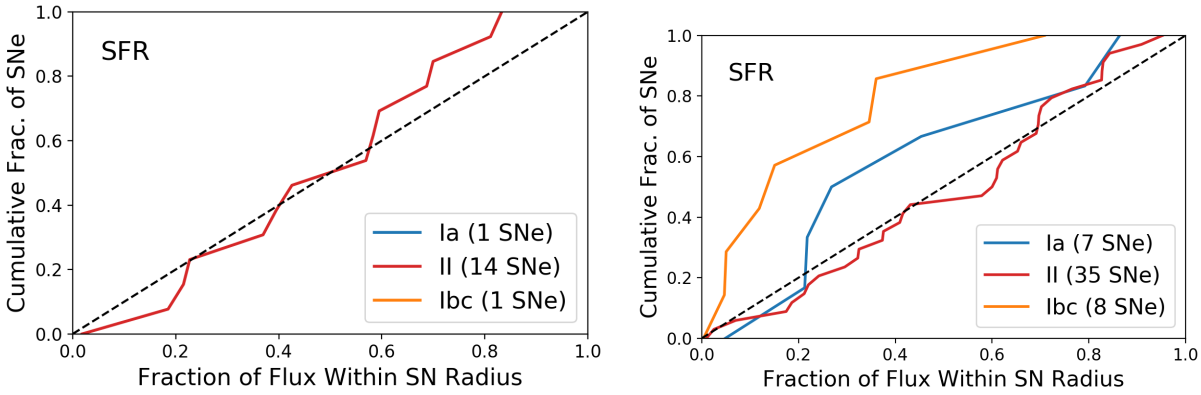

Figure A.3 **0.5 kpc** (left) and **1 kpc** (right) cumulative distributions of SNe Ia (blue), SNe II (red), and SNe Ibc (orange) against the SFR tracer, which is a combination of W4 and FUV light. The dashed diagonal line represents a uniform distribution that traces the IR and UV light of the host galaxies. If a distribution falls above the diagonal line, then that SN type tends to be more radially concentrated than host galaxy emission. If a SN population tends to be more radially extended than its host galaxy emission, then its distribution will fall below the diagonal line. The total count of SNe is 16 for the 0.5 kpc sample and 50 for the 1 kpc sample.

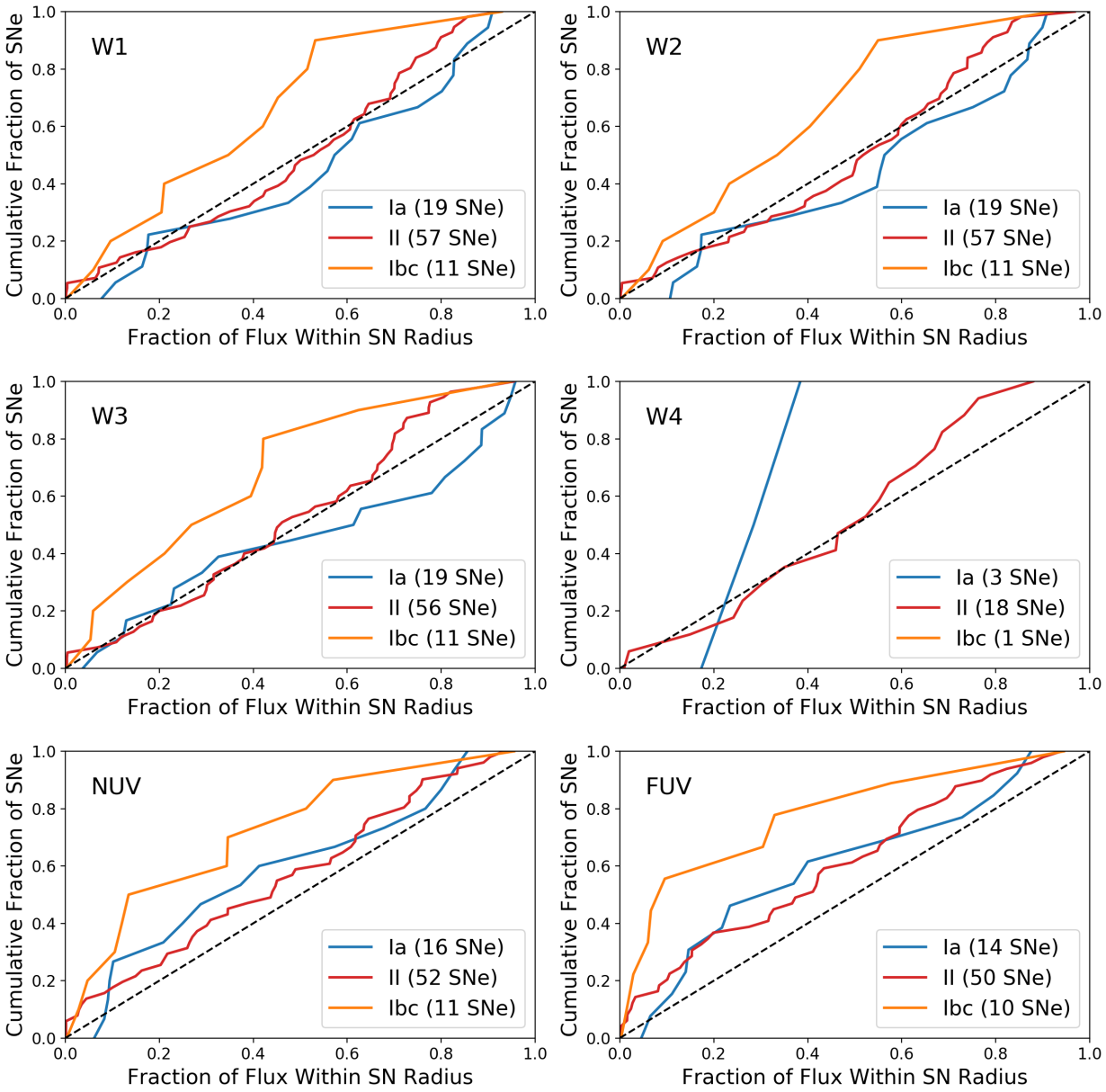

Figure A.4 Cumulative distributions of SNe Ia (blue), SNe II (red), and SNe Ibc (orange) against host galaxy IR (W1, W2, W3, and W4), NUV, and FUV emission within **0.5 kpc** of each SN site. **No selections are made based on inclination**. The dashed diagonal line represents a uniform distribution that traces the IR and UV light of the host galaxies. If a distribution falls above the diagonal line, then that SN type tends to be more radially concentrated than host galaxy emission. If a SN population tends to be more radially extended than its host galaxy emission, then its distribution will fall below the diagonal line.The total sample of SNe is 68 for W1, W2, and W3; 17 for W4; 62 for NUV; and 58 for FUV.

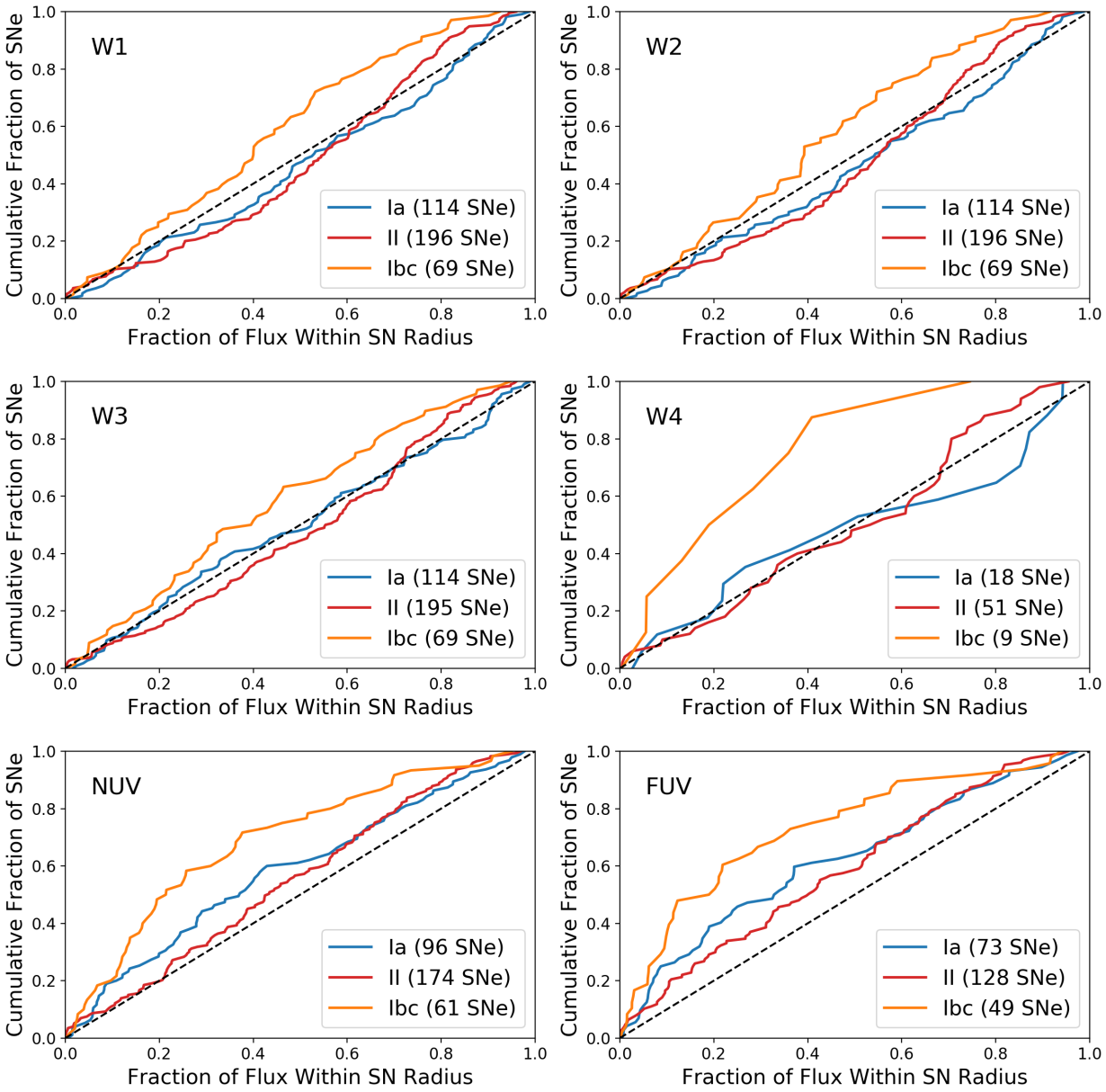

Figure A.5 Cumulative distributions of SNe Ia (blue), SNe II (red), and SNe Ibc (orange) against host galaxy IR (W1, W2, W3, and W4), NUV, and FUV emission within **1 kpc** of each SN site. **No selections are made based on inclination**. The dashed diagonal line represents a uniform distribution that traces the IR and UV light of the host galaxies. If a distribution falls above the diagonal line, then that SN type tends to be more radially concentrated than host galaxy emission. If a SN population tends to be more radially extended than its host galaxy emission, then its distribution will fall below the diagonal line. The total sample of SNe is 320 for W1, W2, and W3; 62 for W4; 276 for NUV; and 209 for FUV.

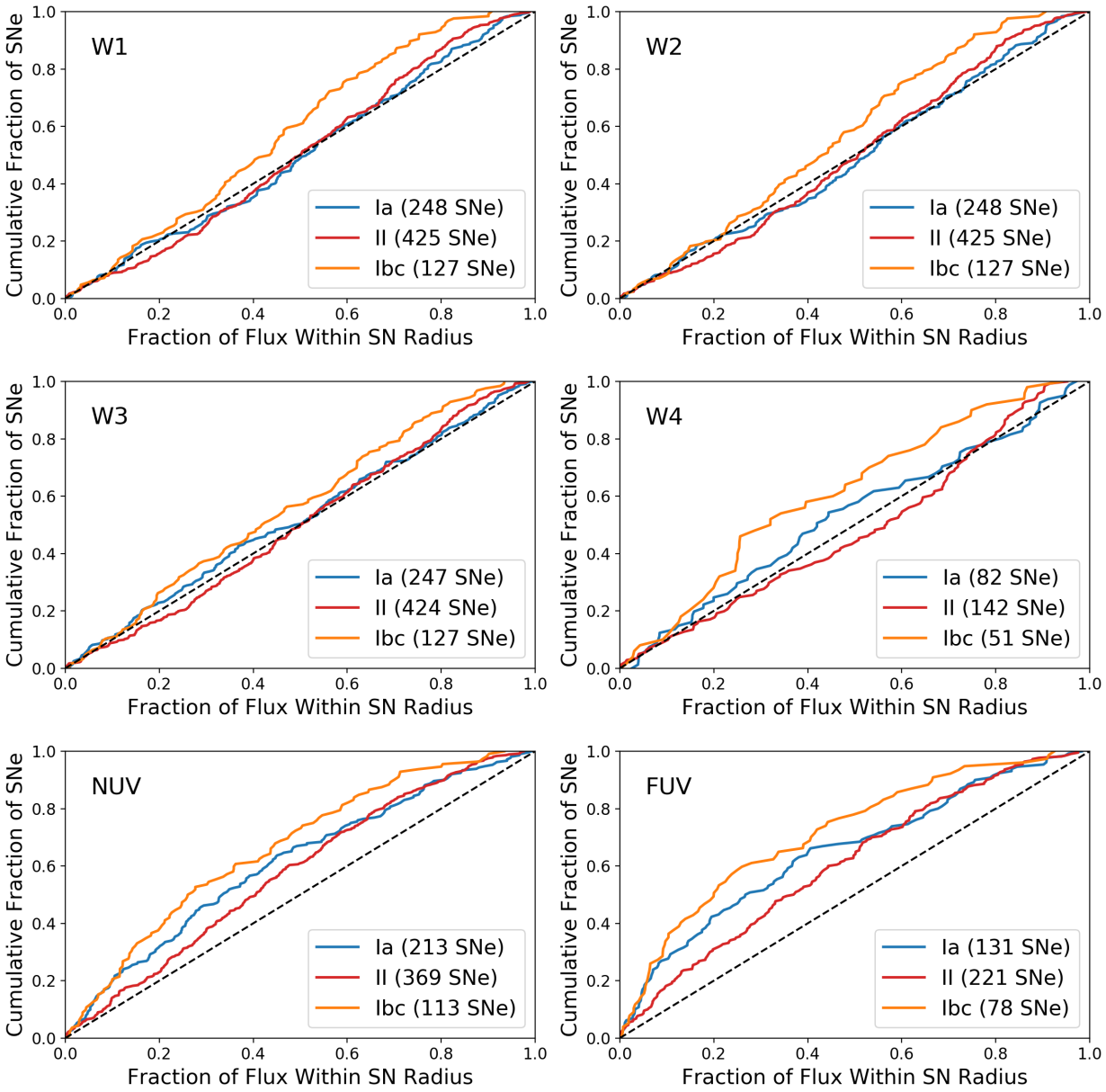

Figure A.6 Cumulative distributions of SNe Ia (blue), SNe II (red), and SNe Ibc (orange) against host galaxy IR (W1, W2, W3, and W4), NUV, and FUV emission within **2 kpc** of each SN site. **No selections are made based on inclination**. The dashed diagonal line represents a uniform distribution that traces the IR and UV light of the host galaxies. If a distribution falls above the diagonal line, then that SN type tends to be more radially concentrated than host galaxy emission. If a SN population tends to be more radially extended than its host galaxy emission, then its distribution will fall below the diagonal line. The total sample of SNe is 687 for W1, W2, and W3; 231 for W4; 599 for NUV; and 371 for FUV.

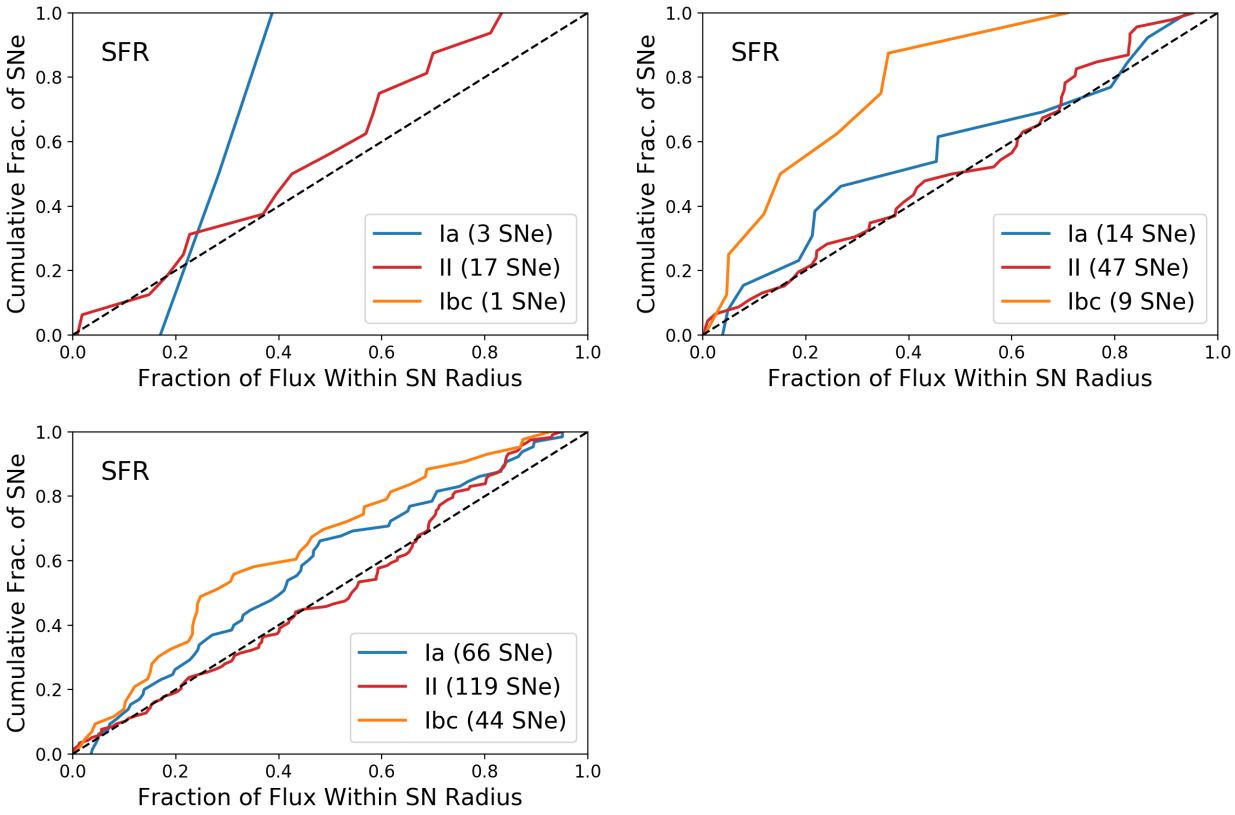

Figure A.7 0.5 kpc (top left), 1 kpc (top right), and 2 kpc (bottom left) cumulative distributions of SNe Ia (blue), SNe II (red), and SNe Ibc (orange) against the SFR tracer, which is a combination of W4 and FUV light. **No selections are made based on inclination**. The dashed diagonal line represents a uniform distribution that traces the IR and UV light of the host galaxies. If a distribution falls above the diagonal line, then that SN type tends to be more radially concentrated than host galaxy emission. If a SN population tends to be more radially extended than its host galaxy emission, then its distribution will fall below the diagonal line. The total count of SNe is 16 for the 0.5 kpc sample, 56 for the 1 kpc sample, and 192 for the 2 kpc sample.

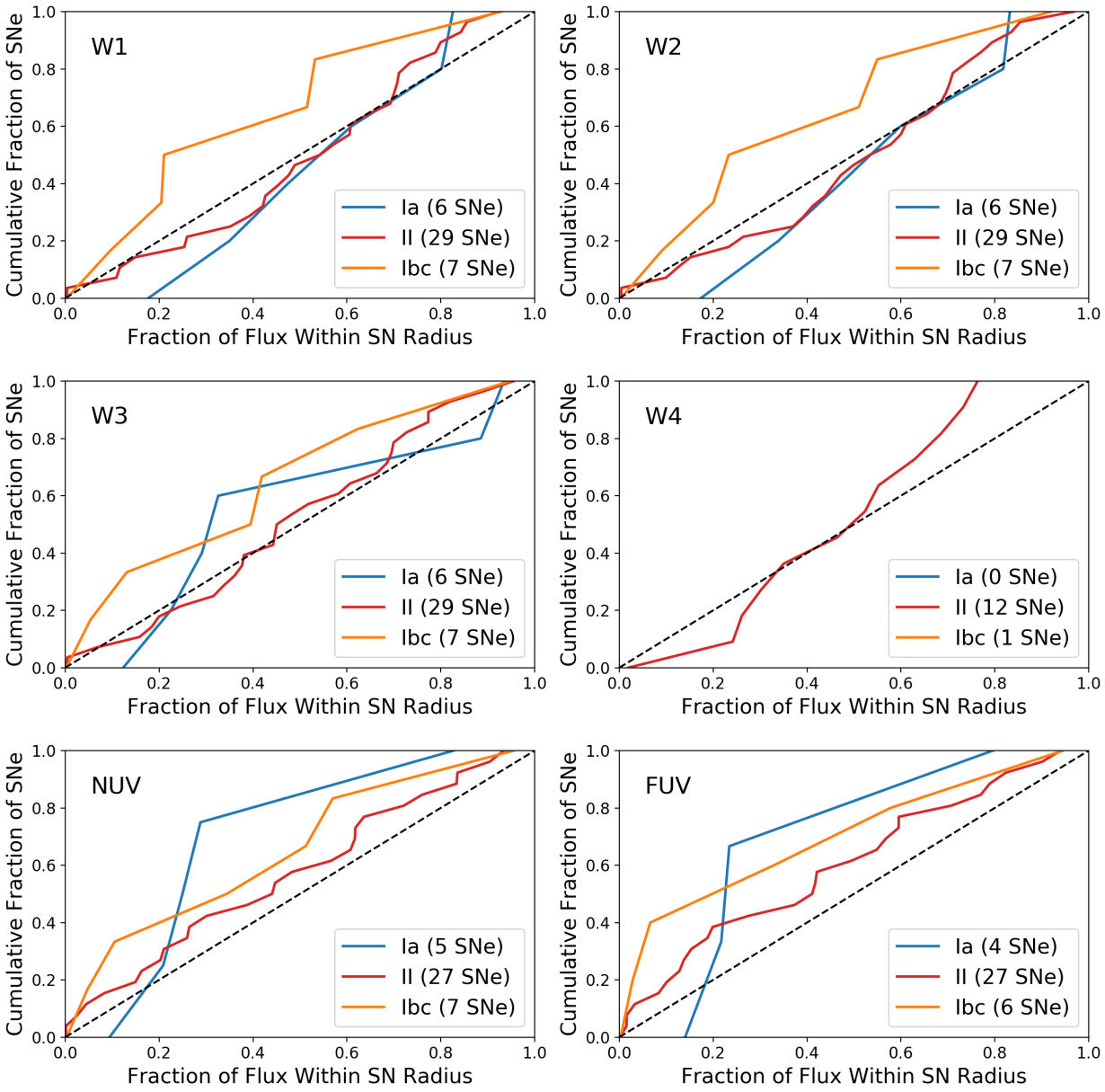

Figure A.8 Cumulative distributions of SNe Ia (blue), SNe II (red), and SNe Ibc (orange) against host galaxy IR (W1, W2, W3, and W4), NUV, and FUV emission within **0.5 kpc** of each SN site. **SNe with discovery dates between 2003 and 2013 (WISE and *GALEX* operations) were removed in order to ensure remaining SN emission was not recorded.** The dashed diagonal line represents a uniform distribution that traces the IR and UV light of the host galaxies. If a distribution falls above the diagonal line, then that SN type tends to be more radially concentrated than host galaxy emission. If a SN population tends to be more radially extended than its host galaxy emission, then its distribution will fall below the diagonal line. The total sample of SNe is 36 for W1, W2, and W3; 10 for W4; 34 for NUV; and 32 for FUV.

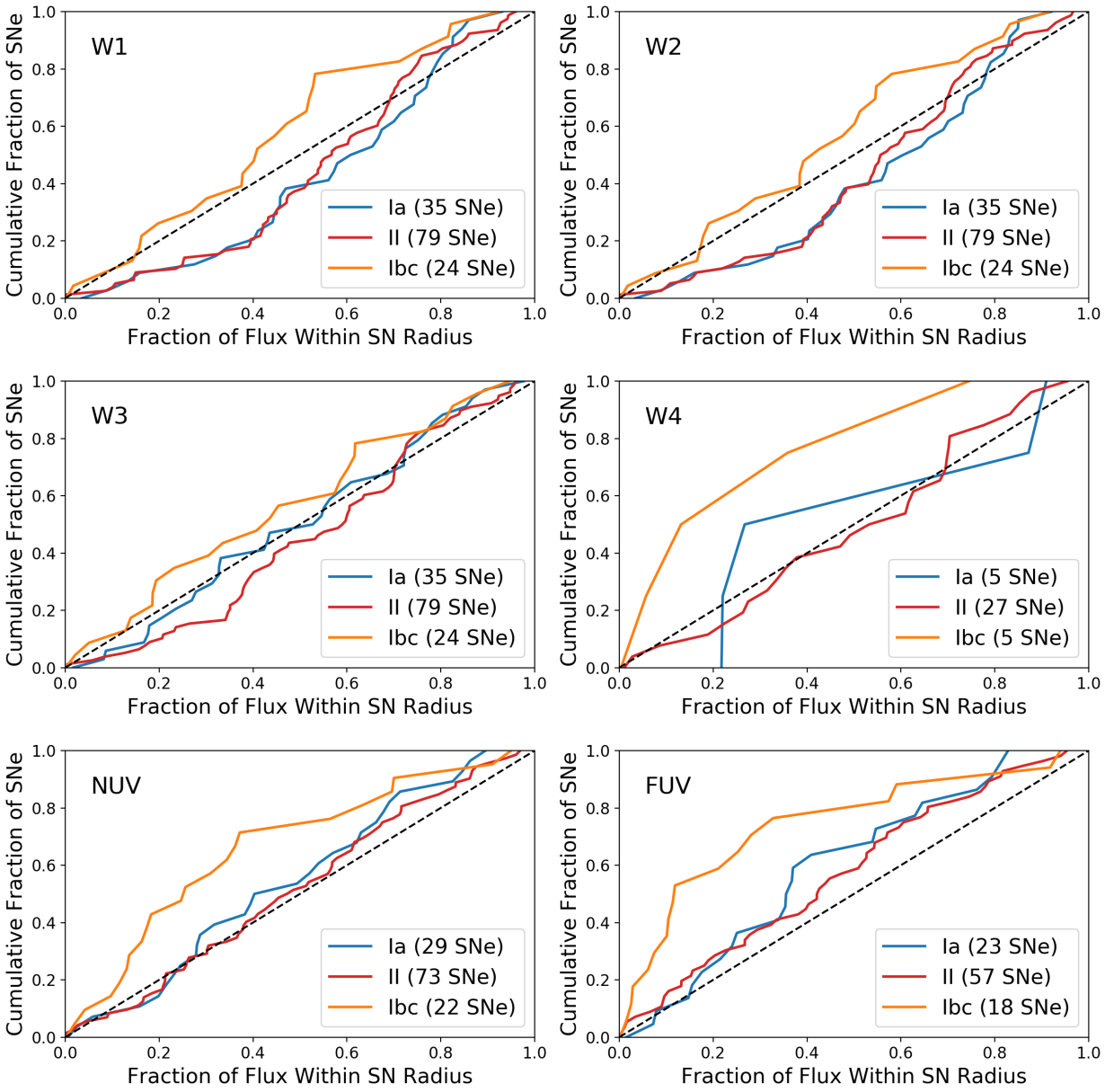

Figure A.9 Cumulative distributions of SNe Ia (blue), SNe II (red), and SNe Ibc (orange) against host galaxy IR (W1, W2, W3, and W4), NUV, and FUV emission within **1 kpc** of each SN site. **SNe with discovery dates between 2003 and 2013 (WISE and *GALEX* operations) were removed in order to ensure remaining SN emission was not recorded.** The dashed diagonal line represents a uniform distribution that traces the IR and UV light of the host galaxies. If a distribution falls above the diagonal line, then that SN type tends to be more radially concentrated than host galaxy emission. If a SN population tends to be more radially extended than its host galaxy emission, then its distribution will fall below the diagonal line. The total sample of SNe is 119 for W1, W2, and W3; 31 for W4; 106 for NUV; and 83 for FUV.

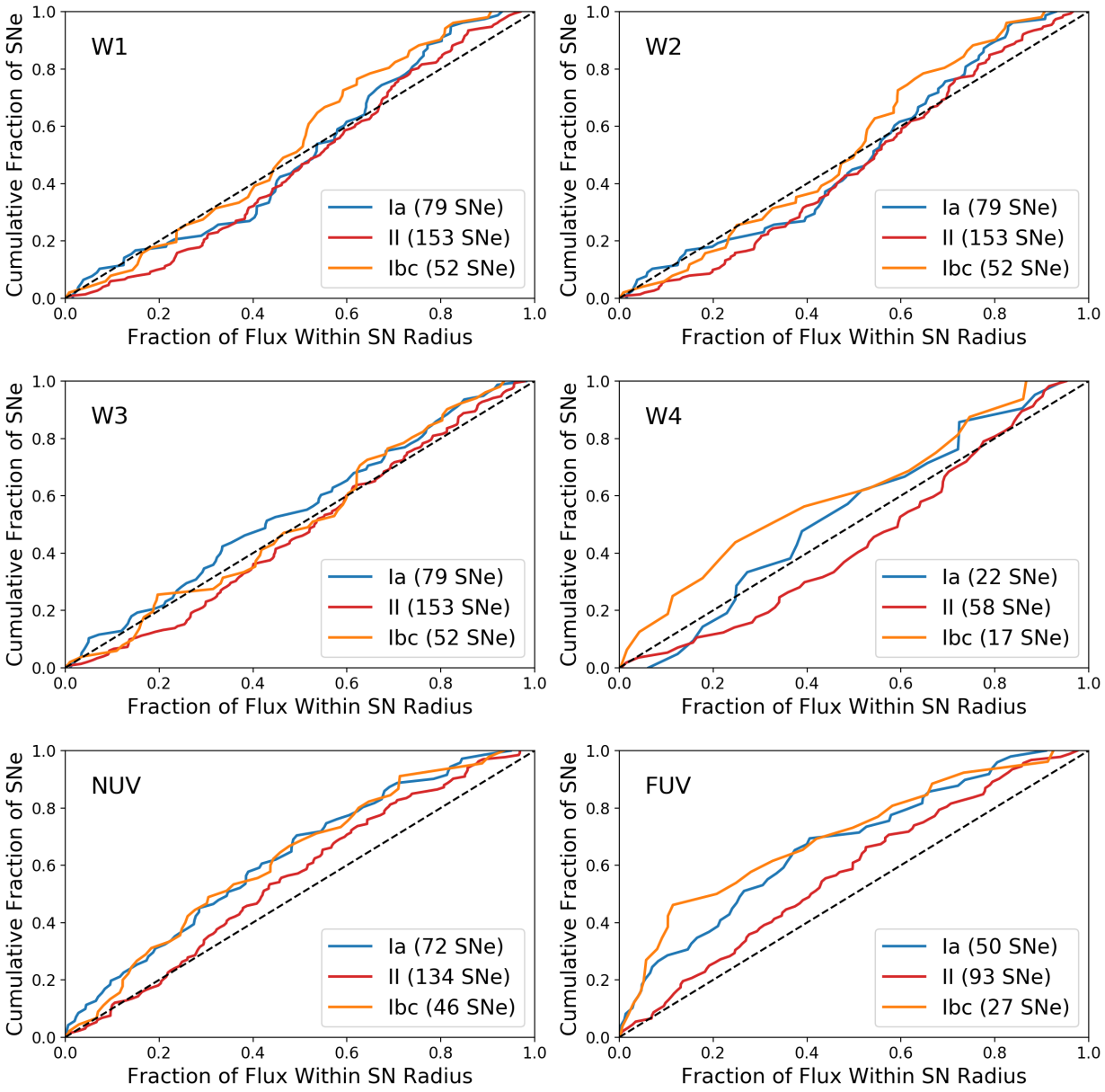

Figure A.10 Cumulative distributions of SNe Ia (blue), SNe II (red), and SNe Ibc (orange) against host galaxy IR (W1, W2, W3, and W4), NUV, and FUV emission within **2 kpc** of each SN site. **SNe with discovery dates between 2003 and 2013 (WISE and *GALEX* operations) were removed in order to ensure remaining SN emission was not recorded.** The dashed diagonal line represents a uniform distribution that traces the IR and UV light of the host galaxies. If a distribution falls above the diagonal line, then that SN type tends to be more radially concentrated than host galaxy emission. If a SN population tends to be more radially extended than its host galaxy emission, then its distribution will fall below the diagonal line. The total sample of SNe is 251 for W1, W2, and W3; 82 for W4; 225 for NUV; and 151 for FUV.

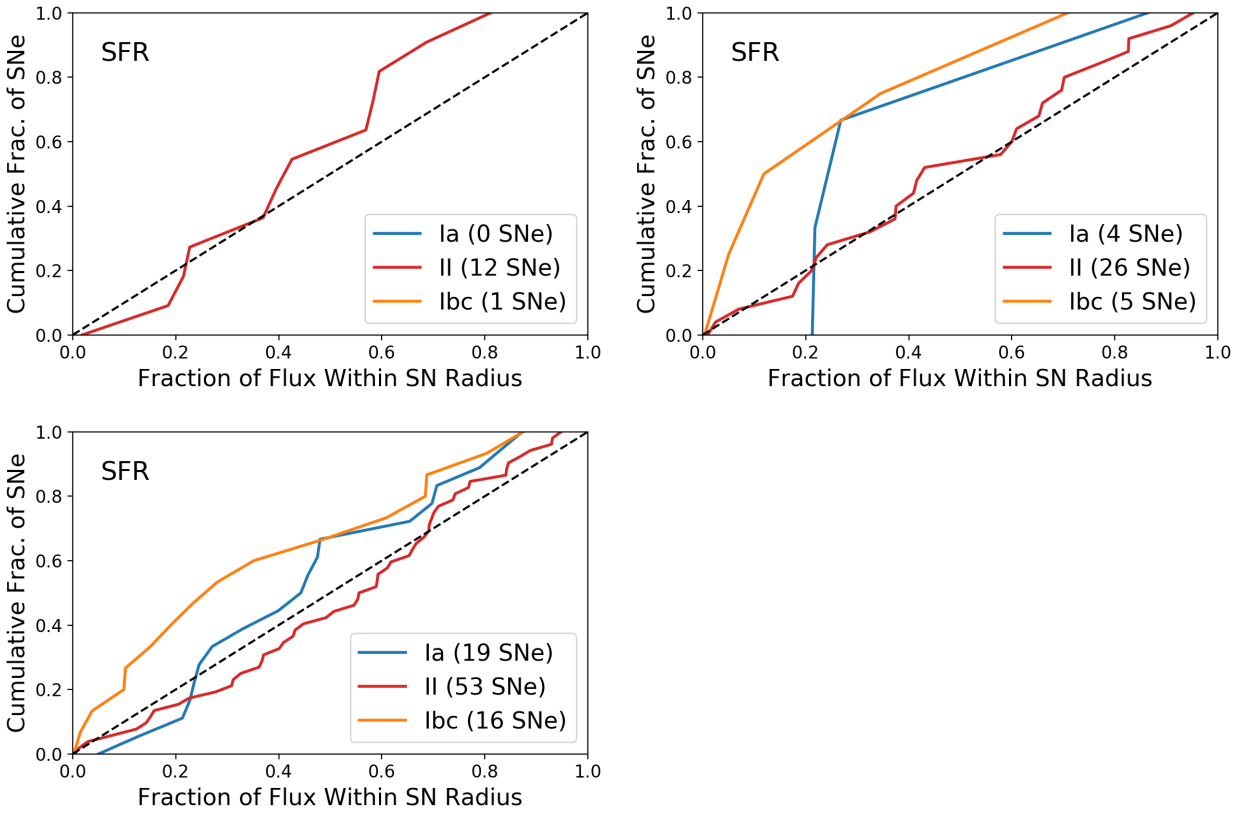

Figure A.11 0.5 kpc (top left), 1 kpc (top right), and 2 kpc (bottom left) cumulative distributions of SNe Ia (blue), SNe II (red), and SNe Ibc (orange) against the SFR tracer, which is a combination of W4 and FUV light. **SNe with discovery dates between 2003 and 2013 (WISE and *GALEX* operations) were removed in order to ensure remaining SN emission was not recorded.** The dashed diagonal line represents a uniform distribution that traces the IR and UV light of the host galaxies. If a distribution falls above the diagonal line, then that SN type tends to be more radially concentrated than host galaxy emission. If a SN population tends to be more radially extended than its host galaxy emission, then its distribution will fall below the diagonal line. The total count of SNe is 10 for the 0.5 kpc sample, 30 for the 1 kpc sample, and 74 for the 2 kpc sample.

Bibliography

Anderson, J. P., Habergham, S. M., James, P. A., and Hamuy, M. (2012). Progenitor mass constraints for core-collapse supernovae from correlations with host galaxy star formation. , 424(2):1372–1391.

Anderson, J. P. and James, P. A. (2008). Constraints on core-collapse supernova progenitors from correlations with Hα emission. , 390(4):1527–1538.

Anderson, J. P. and James, P. A. (2009). Comparisons of the radial distributions of core-collapse supernovae with those of young and old stellar populations. , 399(2):559–573.

Anderson, J. P., James, P. A., Förster, F., González-Gaitán, S., Habergham, S. M., Hamuy, M., and Lyman, J. D. (2015a). On the environments of Type Ia supernovae within host galaxies. , 448(1):732–753.

Anderson, J. P., James, P. A., Habergham, S. M., Galbany, L., and Kuncarayakti, H. (2015b). Statistical Studies of Supernova Environments. , 32:e019.

Anderson, J. P. and Soto, M. (2013). On the multiplicity of supernovae within host galaxies. , 550:A69.

Audcent-Ross, F. M., Meurer, G. R., Audcent, J. R., Ryder, S. D., Wong, O. I., Phan, J., Williamson, A., and Kim, J. H. (2020). The radial distribution of supernovae compared to star formation tracers. , 492(1):848–862.

Crowther, P. A. (2013). On the association between core-collapse supernovae and H ii regions. , 428(3):1927–1943.

Galbany, L., Miquel, R., Östman, L., Brown, P. J., Cinabro, D., D'Andrea, C. B., Frieman, J., Jha, S. W., Marriner, J., Nichol, R. C., Nordin, J., Olmstead, M. D., Sako, M., Schneider, D. P., Smith, M., Sollerman, J., Pan, K., Snedden, S., Bizyaev, D., Brewington, H., Malanushenko, E., Malanushenko, V., Oravetz, D., Simmons, A., and Shelden, A. (2012). Type Ia Supernova Properties as a Function of the Distance to the Host Galaxy in the SDSS-II SN Survey. , 755(2):125.

Galbany, L., Stanishev, V., Mourão, A. M., Rodrigues, M., Flores, H., García-Benito, R., Mast, D., Mendoza, M. A., Sánchez, S. F., Badenes, C., Barrera-Ballesteros, J., Bland-Hawthorn, J., Falcón-Barroso, J., García-Lorenzo, B., Gomes, J. M., González Delgado, R. M., Kehrig, C., Lyubenova, M., López-Sánchez, A. R., de Lorenzo-Cáceres, A., Marino, R. A., Meidt, S., Mollá, M., Papaderos, P., Pérez-Torres, M. A., Rosales-Ortega, F. F., and van de Ven, G. (2014). Nearby supernova host galaxies from the CALIFA Survey. I. Sample, data analysis, and correlation to star-forming regions. , 572:A38.

Guillochon, J., Parrent, J., Kelley, L. Z., and Margutti, R. (2017). An Open Catalog for Supernova Data. , 835(1):64.

Habergham, S. M., Anderson, J. P., and James, P. A. (2010). Type Ibc Supernovae in Disturbed Galaxies: Evidence for a Top-heavy Initial Mass Function. , 717(1):342–347.

Habergham, S. M., James, P. A., and Anderson, J. P. (2012). A central excess of stripped-envelope supernovae within disturbed galaxies. , 424(4):2841–2853.

James, P. A. and Anderson, J. P. (2006). The Hα Galaxy Survey . III. Constraints on supernova progenitors from spatial correlations with Hα emission. , 453(1):57–65.

Kangas, T., Mattila, S., Kankare, E., Kotilainen, J. K., Väisänen, P., Greimel, R., and Takalo, A. (2013). Spatial distributions of core-collapse supernovae in infrared-bright galaxies. , 436(4):3464–3479.

Kelly, P. L., Kirshner, R. P., and Pahre, M. (2008). Long γ-Ray Bursts and Type Ic Core-Collapse Supernovae Have Similar Locations in Hosts. , 687(2):1201–1207.

Leroy, A. K., Sandstrom, K. M., Lang, D., Lewis, A., Salim, S., Behrens, E. A., Chastenet, J., Chiang, I. D., Gallagher, M. J., Kessler, S., and Utomo, D. (2019). A z = 0 Multiwavelength Galaxy Synthesis. I. A WISE and GALEX Atlas of Local Galaxies. , 244(2):24.

Makarov, D., Prugniel, P., Terekhova, N., Courtois, H., and Vauglin, I. (2014). HyperLEDA. III. The catalogue of extragalactic distances. , 570:A13.

Martin, D. C., Fanson, J., Schiminovich, D., Morrissey, P., Friedman, P. G., Barlow, T. A., Conrow, T., Grange, R., Jelinsky, P. N., Milliard, B., Siegmund, O. H. W., Bianchi, L., Byun, Y.-I., Donas, J., Forster, K., Heckman, T. M., Lee, Y.-W., Madore, B. F., Malina, R. F., Neff, S. G., Rich, R. M., Small, T., Surber, F., Szalay, A. S., Welsh, B., and Wyder, T. K. (2005). The Galaxy Evolution Explorer: A Space Ultraviolet Survey Mission. , 619(1):L1–L6.

Wright, E. L., Eisenhardt, P. R. M., Mainzer, A. K., Ressler, M. E., Cutri, R. M., Jarrett, T., Kirkpatrick, J. D., Padgett, D., McMillan, R. S., Skrutskie, M., Stanford, S. A., Cohen, M., Walker, R. G., Mather, J. C., Leisawitz, D., Gautier, Thomas N., I., McLean, I., Benford, D., Lonsdale, C. J., Blain, A., Mendez, B., Irace, W. R., Duval, V., Liu, F., Royer, D., Heinrichsen, I., Howard, J., Shannon, M., Kendall, M., Walsh, A. L., Larsen, M., Cardon, J. G., Schick, S., Schwalm, M., Abid, M., Fabinsky, B., Naes, L., and Tsai,

C.-W. (2010). The Wide-field Infrared Survey Explorer (WISE): Mission Description and Initial On-orbit Performance. , 140(6):1868–1881.